Chapter 3
The Helmholtz Equation Least-Squares Method

In engineering applications, most vibrating surfaces are of arbitrary shapes. Moreover, the environments are often nonideal such that the radiated acoustic pressure field cannot be solved by any analytic methods, including expansion theories. Therefore, approximate solutions are sought. The Helmholtz equation least-squares (HELS) method [36, 37] offers such approximate solutions to a wide variety of acoustic radiation problems encountered in practice. Note that HELS can not only be used to reconstruct but also to predict the radiated acoustic field emitted by an arbitrarily shaped vibrating body.

If Fourier transform-based NAH is the first generation and BEM-based NAH the second in the evolution of NAH technology because of their respective significance, the third generation would be HELS-based NAH. Unlike the first two generations, HELS-based NAH does not seek analytic solutions to the acoustic fields generated by arbitrarily shaped structures that cannot be found anyway. Rather, it attempts to find the best approximation of an acoustic field through an expansion of certain basis functions. This approach greatly simplifies reconstruction, yet enables one to tackle a complex problem involving an arbitrarily shaped surface in a non-free field with fewer measurement points than both the Fourier transform and BEM-based NAH do. This makes HELS potentially a practical and versatile tool for diagnosing noise and vibration problems.

The development of HELS method started in the mid-1990s. In HELS the acoustic pressure is written as an expansion of the particular solution to the Helmholtz equation. Using the spherical coordinates, the particular solution is expressible as the spherical wave functions. The coefficients associated with the expansion functions can be determined by solving an overdetermined linear system of equations obtained by matching the assumed-form solution to the measured acoustic pressures, and the errors incurred in this process are minimized by the least-squares method.

S.F. Wu, *The Helmholtz Equation Least Squares Method*, Modern Acoustics and Signal Processing, DOI 10.1007/978-1-4939-1640-5_3

3.1 The HELS Formulations

To put it simply, the HELS method uses an expansion of some basis functions to describe the acoustic pressure generated by an arbitrary source anywhere. The requirements on the basis functions are that they must satisfy the Helmholtz equation and are bounded. Therefore different basis functions may be used, depending on whether the region in which the HELS solution is intended for is external or internal to a source surface. There is no restriction whatsoever on the choice of coordinate system, but the rule of thumb is that for a blunt object whose aspect ratio is close to (1:1:1), then the spherical coordinate system is a natural choice. Similarly, for an elongated object whose aspect ratio is close to (1:1:10), the prolate coordinate would be ideal, and for a discoidal object whose aspect ratio is close to (1:10:10), the oblate would be best. In the matrix form, the HELS formulation can be expressed as follows:

$$\left\{\hat{p}\left(\vec{x};\omega\right)\right\} = \left[\Psi^{(1)}\left(\vec{x};\omega\right)\right]\{C(\omega)\}, \tag{3.1}$$

where $\hat{p}\left(\vec{x};\omega\right)$ implies the complex amplitude of the acoustic pressure at any field point $\vec{x}$, and $\Psi_{ij}^{(1)}\left(\vec{x};\omega\right)$ are the particular solutions to the Helmholtz equation. Using the spherical coordinates, one can write $\Psi_{ij}^{(1)}\left(\vec{x};\omega\right)$ as

$$\Psi_{ij}^{(1)}\left(\vec{x};\omega\right) \equiv \Psi_{nl}^{(1)}(r,\theta,\phi;\omega) = h_n^{(1)}(kr)Y_n^l(\theta,\phi), \tag{3.2}$$

where the first index i in $\Psi_{ij}^{(1)}\left(\vec{x};\omega\right)$ indicates the ith reconstruction point and the second index j implies the jth term of expansion functions. When the spherical coordinates are used, these indices can be replaced by n and l, where n is associated with the radial functions and l is with the angular functions. The indices j, n, and l in Eq. (3.2) are related via $j = n^2 + n + l + 1$ with n starting from 0 to N and l from $-n$ to $+n$. $\Psi_{ij}^{(1)}\left(\vec{x};\omega\right)$ are orthogonal with respect to the angular coordinates

$$\begin{aligned}&\int_0^{2\pi} d\phi \int_0^{\pi} \Psi_{n'l'}^{(1)}(r,\theta,\phi;\omega)\Psi_{nl}^{(1)*}(r,\theta,\phi;\omega)\sin\theta d\theta \\ &\quad = h_{n'}^{(1)}(kr)h_n^{(1)*}(kr)\int_0^{2\pi} d\phi \int_0^{\pi} Y_{n'}^{l'}(\theta,\phi)Y_n^{l*}(\theta,\phi)\sin\theta d\theta = h_{n'}^{(1)}(kr)h_n^{(1)*}(kr)\delta_{n'n}\delta_{m'm}.\end{aligned} \tag{3.3}$$

From Chap. 2 we have learned that the expansion functions $\Psi_{ij}^{(1)}\left(\vec{x};\omega\right)$ form a complete basis from which any function defined on a spherical surface can be uniquely represented.

Using the spherical Hankel functions and spherical harmonics given in Examples 2.1 and 2.9, we can write the first few terms ($n=0$, 1, 2) of the expansion functions $\Psi_{ij}^{(1)}\left(\vec{x};\omega\right)$ as follows:

For $n=0$,

$$\Psi_{i1}^{(1)}(r,\theta,\phi;\omega) = -i\frac{1}{2\sqrt{\pi}}\frac{\mathrm{e}^{ikr}}{kr}. \tag{3.4}$$

For $n=1$,

$$\Psi_{i2}^{(1)}(r,\theta,\phi;\omega) = -\frac{1}{2}\sqrt{\frac{3}{\pi}}\frac{(kr+i)\cos\theta}{(kr)^2}\mathrm{e}^{ikr}, \tag{3.5}$$

$$\Psi_{i3}^{(1)}(r,\theta,\phi;\omega) = -\frac{1}{2}\sqrt{\frac{3}{2\pi}}\frac{(kr+i)\sin\theta}{(kr)^2}\mathrm{e}^{i(kr-\phi)}, \tag{3.6}$$

$$\Psi_{i4}^{(1)}(r,\theta,\phi;\omega) = \frac{1}{2}\sqrt{\frac{3}{2\pi}}\frac{(kr+i)\sin\theta}{(kr)^2}\mathrm{e}^{i(kr+\phi)}. \tag{3.7}$$

For $n=2$,

$$\Psi_{i5}^{(1)}(r,\theta,\phi;\omega) = i\frac{1}{4}\sqrt{\frac{5}{\pi}}\frac{\left[(kr)^2-3+i3(kr)\right](3\cos^2\theta-1)}{(kr)^3}\mathrm{e}^{i(kr+\phi)}, \tag{3.8}$$

$$\Psi_{i6}^{(1)}(r,\theta,\phi;\omega) = i\frac{3}{2}\sqrt{\frac{5}{6\pi}}\frac{\left[(kr)^2-3+i3(kr)\right]\sin\theta\cos\theta}{(kr)^3}\mathrm{e}^{i(kr-\phi)}, \tag{3.9}$$

$$\Psi_{i7}^{(1)}(r,\theta,\phi;\omega) = -i\frac{3}{2}\sqrt{\frac{5}{6\pi}}\frac{\left[(kr)^2-3+i3(kr)\right]\sin\theta\cos\theta}{(kr)^3}\mathrm{e}^{i(kr+\phi)}, \tag{3.10}$$

$$\Psi_{i8}^{(1)}(r,\theta,\phi;\omega) = i\frac{3}{4}\sqrt{\frac{5}{6\pi}}\frac{\left[(kr)^2-3+i3(kr)\right]\sin^2\theta}{(kr)^3}\mathrm{e}^{i(kr-2\phi)}, \tag{3.11}$$

$$\Psi_{i9}^{(1)}(r,\theta,\phi;\omega) = i\frac{3}{4}\sqrt{\frac{5}{6\pi}}\frac{\left[(kr)^2-3+i3(kr)\right]\sin^2\theta}{(kr)^3}\mathrm{e}^{i(kr+2\phi)}. \tag{3.12}$$

Physically, the $n=0$ term (3.4) represents a monopole source, the $n=1$ terms (3.5)–(3.7) depict the effects of three dipole sources in three mutually orthogonal axes directions, and $n=2$ terms (3.8)–(3.11) describe the effects of five quadrupole sources, for which the terms given by Eqs. (3.8)–(3.10) portray the effects of longitudinal quadrupoles, and those given by Eqs. (3.11) and (3.12) describe the effects of lateral quadrupoles. In general the number of terms in the nth index is $(2n+1)$ and that of total expansion terms is $J=(n+1)^2$.

The coefficients $\{C(\omega)\}$ associated with the expansion functions are obtained by matching Eq. (3.1) to the measured acoustic pressures $\hat{p}\left(\vec{x}_m^{\,\text{meas}};\omega\right)$ at $\vec{x}_m^{\,\text{meas}}$ on the hologram surface, where $m=1$ to M, J indicates the number of basis functions, and M the number of measurement points. In practice we take more measurement points than the number of expansion terms, $M>J$. Hence Eq. (3.1) becomes an overdetermined set of equations for the coefficients $\{C(\omega)\}$,

$$\left\{\hat{p}\left(\vec{x}_m^{\,\text{meas}};\omega\right)\right\}_{M\times 1}=\left[\Psi\left(\vec{x}_m^{\,\text{meas}};\omega\right)\right]_{M\times J}\{C(\omega)\}_{J\times 1}. \tag{3.13}$$

Solving Eq. (3.13) by taking a pseudo inversion, we obtain

$$\begin{aligned}\{C(\omega)\}_{J\times 1}=&\left(\left[\Psi\left(\vec{x}_m^{\,\text{meas}};\omega\right)\right]_{J\times M}^{H}\left[\Psi\left(\vec{x}_m^{\,\text{meas}};\omega\right)\right]_{M\times J}\right)^{-1}\\&\left[\Psi\left(\vec{x}_m^{\,\text{meas}};\omega\right)\right]_{J\times M}^{H}\left\{\hat{p}\left(\vec{x}_m^{\,\text{meas}};\omega\right)\right\}_{M\times 1},\end{aligned} \tag{3.14}$$

where the superscript H represents Hermitian transpose.

Once the expansion coefficients are specified, the acoustic pressure at $\vec{x}_S^{\,\text{rec}}$ on the source surface can be reconstructed by substituting Eq. (3.14) into (3.1),

$$\left\{\hat{p}\left(\vec{x}_s^{\,\text{rec}};\omega\right)\right\}_{S\times 1}=\left[G_{pp}\left(\vec{x}_s^{\,\text{rec}}\middle|\vec{x}_m^{\,\text{meas}};\omega\right)\right]_{S\times M}\left\{\hat{p}\left(\vec{x}_m^{\,\text{meas}};\omega\right)\right\}_{M\times 1}, \tag{3.15}$$

where $\left[G_{pp}\left(\vec{x}_s^{\,\text{rec}}\middle|\vec{x}_m^{\,\text{meas}};\omega\right)\right]_{S\times M}$ represents the transfer matrix that correlates the measured acoustic pressure at $\vec{x}_m^{\,\text{meas}}$ to the reconstructed acoustic pressure at $\vec{x}_S^{\,\text{rec}}$,

$$\begin{aligned}\left[G_{pp}\left(\vec{x}_s^{\,\text{rec}}\middle|\vec{x}_m^{\,\text{meas}};\omega\right)\right]_{S\times M}=&\left[\Psi\left(\vec{x}_s^{\,\text{rec}};\omega\right)\right]_{S\times J}\left(\left[\Psi\left(\vec{x}_m^{\,\text{meas}};\omega\right)\right]_{J\times M}^{H}\left[\Psi\left(\vec{x}_m^{\,\text{meas}};\omega\right)\right]_{M\times J}\right)^{-1}\\&\left[\Psi\left(\vec{x}_m^{\,\text{meas}};\omega\right)\right]_{J\times M}^{H}.\end{aligned} \tag{3.16}$$

The normal component of the surface velocity $\hat{v}_{\text{n}}\left(\vec{x}_s^{\,\text{rec}};\omega\right)$ can be obtained from Eq. (3.15) by using the Euler's equation,

$$\left\{\hat{v}_{\mathrm{n}}\left(\vec{x}_s^{\,\mathrm{rec}};\omega\right)\right\}_{S\times 1}=\left[G_{pv}\left(\vec{x}_s^{\,\mathrm{rec}}\middle|\vec{x}_m^{\,\mathrm{meas}};\omega\right)\right]_{S\times M}\left\{\hat{p}\left(\vec{x}_m^{\,\mathrm{meas}};\omega\right)\right\}_{M\times 1},\tag{3.17}$$

where $\left[G_{pv}\left(\vec{x}_s^{\,\mathrm{rec}}\middle|\vec{x}_m^{\,\mathrm{meas}};\omega\right)\right]_{S\times M}$ represents the transfer matrix that correlates the measured acoustic pressure at $\vec{x}_m^{\,\mathrm{meas}}$ to the reconstructed normal surface velocity at $\vec{x}_S^{\,\mathrm{rec}}$,

$$\begin{aligned}\left[G_{pv}\left(\vec{x}_s^{\,\mathrm{rec}}\middle|\vec{x}_m^{\,\mathrm{meas}};\omega\right)\right]_{S\times M}=&\frac{1}{i\omega\rho_0}\left[\frac{\partial\Psi\left(\vec{x}_s^{\,\mathrm{rec}};\omega\right)}{\partial \mathrm{n}}\right]_{S\times J}\\&\left(\left[\Psi\left(\vec{x}_m^{\,\mathrm{meas}};\omega\right)\right]_{J\times M}^{H}\left[\Psi\left(\vec{x}_m^{\,\mathrm{meas}};\omega\right)\right]_{M\times J}\right)^{-1}\left[\Psi\left(\vec{x}_m^{\,\mathrm{meas}};\omega\right)\right]_{J\times M}^{H}.\end{aligned}\tag{3.18}$$

Once $\hat{p}\left(\vec{x}_m^{\,meas};\omega\right)$ and $\hat{v}_{\mathrm{n}}\left(\vec{x}_s^{\,\mathrm{rec}};\omega\right)$ are reconstructed, the normal component of the time-averaged acoustic intensity on the source surface can be calculated as

$$\left\{\hat{I}_{av,\mathrm{n}}\left(\vec{x}_s^{\,\mathrm{rec}};\omega\right)\right\}_{S\times 1}=\frac{1}{2}\mathrm{Re}\left\{\hat{p}\left(\vec{x}_s^{\,\mathrm{rec}};\omega\right)\hat{v}_{\mathrm{n}}^{*}\left(\vec{x}_s^{\,\mathrm{rec}};\omega\right)\right\}_{S\times 1}.\tag{3.19}$$

The radiated acoustic power can be obtained by integrating the normal component of the time-averaged acoustic intensity over the source surface,

$$\mathbf{P}_{av}(\omega)=\iint_S \hat{I}_{av,\mathrm{n}}\left(\vec{x}_s^{\,\mathrm{rec}};\omega\right)dS.\tag{3.20}$$

Therefore all acoustic quantities generated by this source are completely determined.

3.2 Reconstructing the Radiated Acoustic Field

Now let us use the HELS formulation (3.1) to reconstruct the acoustic pressures based on the measurements taken on a hologram surface surround a vibrating object.

Example 3.1 For simplicity yet without loss of generality, let us consider a vibrating sphere of the radius $r=a$ at a constant frequency f. Suppose that the acoustic pressures on a spherical hologram surface Γ of radius $r=r_m^{\mathrm{meas}}$ are taken and the acoustic pressures anywhere in the field including the vibrating surface are

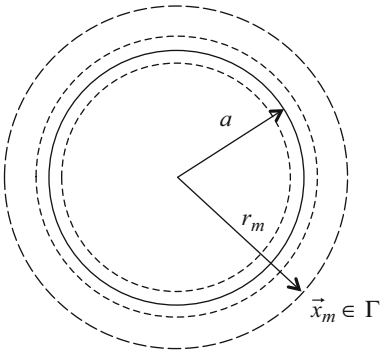

Fig. 3.1 Schematic of reconstructing the acoustic field generated by a dilating sphere around radius $r = a$ using HELS-based NAH. The measured acoustic pressures are taken on a concentric spherical surface of radius r_m

sought (see Fig. 3.1). To illustrate the use of Eq. (3.1), we assume that the number of measurements and that of reconstruction points be equal and set $S = M = 2$, and the reconstructed acoustic pressures are set to equal to the measured ones.

$$\begin{Bmatrix} \hat{p}\left(r_1^{\text{meas}}, \theta_1^{\text{meas}}, \phi_1^{\text{meas}}; \omega\right) \\ \hat{p}\left(r_2^{\text{meas}}, \theta_2^{\text{meas}}, \phi_2^{\text{meas}}; \omega\right) \end{Bmatrix}_{2\times 1}$$

$$= \begin{bmatrix} \Psi_{11}^{(1)}\left(r_1^{\text{meas}}, \theta_1^{\text{meas}}, \phi_1^{\text{meas}}; \omega\right) & \Psi_{12}^{(1)}\left(r_1^{\text{meas}}, \theta_1^{\text{meas}}, \phi_1^{\text{meas}}; \omega\right) \\ \Psi_{21}^{(1)}\left(r_2^{\text{meas}}, \theta_2^{\text{meas}}, \phi_2^{\text{meas}}; \omega\right) & \Psi_{22}^{(1)}\left(r_2^{\text{meas}}, \theta_2^{\text{meas}}, \phi_2^{\text{meas}}; \omega\right) \end{bmatrix}_{2\times 2} \begin{Bmatrix} C_1(\omega) \\ C_2(\omega) \end{Bmatrix}_{2\times 1},$$

where $\Psi_{ij}^{(1)}(r_i^{\text{meas}}, \theta_i^{\text{meas}}, \phi_i^{\text{meas}}; \omega)$ are given by

$$\Psi_{11}^{(1)}\left(r_1^{\text{meas}}, \theta_1^{\text{meas}}, \phi_1^{\text{meas}}; \omega\right) = -i\frac{1}{2\sqrt{\pi}}\frac{\mathrm{e}^{ikr_1^{\text{meas}}}}{kr_1^{\text{meas}}},$$

$$\Psi_{12}^{(1)}\left(r_1^{\text{meas}}, \theta_1^{\text{meas}}, \phi_1^{\text{meas}}; \omega\right) = -\frac{1}{2}\sqrt{\frac{3}{\pi}}\frac{\left(kr_1^{\text{meas}} + i\right)\cos\theta_1^{\text{meas}}}{\left(kr_1^{\text{meas}}\right)^2}\mathrm{e}^{ikr_1^{\text{meas}}},$$

$$\Psi_{21}^{(1)}\left(r_2^{\text{meas}}, \theta_2^{\text{meas}}, \phi_2^{\text{meas}}; \omega\right) = -i\frac{1}{2\sqrt{\pi}}\frac{\mathrm{e}^{ikr_2^{\text{meas}}}}{kr_2^{\text{meas}}},$$

$$\Psi_{22}^{(1)}\left(r_2^{\text{meas}}, \theta_2^{\text{meas}}, \phi_2^{\text{meas}}; \omega\right) = -\frac{1}{2}\sqrt{\frac{3}{\pi}}\frac{\left(kr_2^{\text{meas}} + i\right)\cos\theta_2^{\text{meas}}}{\left(kr_2^{\text{meas}}\right)^2}\mathrm{e}^{ikr_2^{\text{meas}}}.$$

The expansion coefficients $\{C(\omega)\}$ can be determined by inverting the square matrix directly:

$$\begin{Bmatrix} C_1(\omega) \\ C_2(\omega) \end{Bmatrix}_{2\times 1} = \begin{bmatrix} \Psi_{11}^{(1)}\left(r_1^{\text{meas}},\theta_1^{\text{meas}},\phi_1^{\text{meas}};\omega\right) & \Psi_{12}^{(1)}\left(r_1^{\text{meas}},\theta_1^{\text{meas}},\phi_1^{\text{meas}};\omega\right) \\ \Psi_{21}^{(1)}\left(r_2^{\text{meas}},\theta_2^{\text{meas}},\phi_2^{\text{meas}};\omega\right) & \Psi_{22}^{(1)}\left(r_2^{\text{meas}},\theta_2^{\text{meas}},\phi_2^{\text{meas}};\omega\right) \end{bmatrix}_{2\times 2}^{-1}$$

$$\begin{Bmatrix} \hat{p}\left(r_1^{\text{meas}},\theta_1^{\text{meas}},\phi_1^{\text{meas}};\omega\right) \\ \hat{p}\left(r_2^{\text{meas}},\theta_2^{\text{meas}},\phi_2^{\text{meas}};\omega\right) \end{Bmatrix}_{2\times 1}$$

$$= \frac{1}{\det\left[\Psi^{(1)}(r,\theta,\phi;\omega)\right]} \begin{bmatrix} \Psi_{22}^{(1)}\left(r_2^{\text{meas}},\theta_2^{\text{meas}},\phi_2^{\text{meas}};\omega\right) & -\Psi_{12}^{(1)}\left(r_1^{\text{meas}},\theta_1^{\text{meas}},\phi_1^{\text{meas}};\omega\right) \\ -\Psi_{21}^{(1)}\left(r_2^{\text{meas}},\theta_2^{\text{meas}},\phi_2^{\text{meas}};\omega\right) & \Psi_{11}^{(1)}\left(r_1^{\text{meas}},\theta_1^{\text{meas}},\phi_1^{\text{meas}};\omega\right) \end{bmatrix}_{2\times 2}$$

$$\begin{Bmatrix} \hat{p}\left(r_1^{\text{meas}},\theta_1^{\text{meas}},\phi_1^{\text{meas}};\omega\right) \\ \hat{p}\left(r_2^{\text{meas}},\theta_2^{\text{meas}},\phi_2^{\text{meas}};\omega\right) \end{Bmatrix}_{2\times 1},$$

where the determinant of the transfer matrix is given by

$$\det\left[\Psi^{(1)}(r,\theta,\phi;\omega)\right]$$

$$= \Psi_{11}^{(1)}\left(r_1^{\text{meas}},\theta_1^{\text{meas}},\phi_1^{\text{meas}};\omega\right)\Psi_{22}^{(1)}\left(r_2^{\text{meas}},\theta_2^{\text{meas}},\phi_2^{\text{meas}};\omega\right)$$

$$-\Psi_{12}^{(1)}\left(r_1^{\text{meas}},\theta_1^{\text{meas}},\phi_1^{\text{meas}};\omega\right)\Psi_{21}^{(1)}\left(r_2^{\text{meas}},\theta_2^{\text{meas}},\phi_2^{\text{meas}};\omega\right).$$

$$= \frac{\sqrt{3}e^{ik\left(r_1^{\text{meas}}+r_2^{\text{meas}}\right)}}{4\pi}\left[\frac{r_2^{\text{meas}}\left(1-ikr_1^{\text{meas}}\right)\cos\theta_1^{\text{meas}} - r_1^{\text{meas}}\left(1-ikr_2^{\text{meas}}\right)\cos\theta_2^{\text{meas}}}{k^3\left(r_1^{\text{meas}}r_2^{\text{meas}}\right)^2}\right]$$

Substituting the determinant and $\Psi_{ij}^{(1)}(r_i,\theta_i,\phi_i;\omega)$ into the elements of $\{C(\omega)\}$, we obtain

$$\frac{\Psi_{22}^{(1)}\left(r_2^{\text{meas}},\theta_2^{\text{meas}},\phi_2^{\text{meas}};\omega\right)}{\det\left[\Psi^{(1)}(r,\theta,\phi;\omega)\right]} = -\frac{2\sqrt{\pi}k\left(r_1^{\text{meas}}\right)^2\left(kr_2^{\text{meas}}+i\right)\cos\theta_2^{\text{meas}}e^{-ikr_1^{\text{meas}}}}{r_2^{\text{meas}}\left(1-ikr_1^{\text{meas}}\right)\cos\theta_1^{\text{meas}} - r_1^{\text{meas}}\left(1-ikr_2^{\text{meas}}\right)\cos\theta_2^{\text{meas}}},$$

$$-\frac{\Psi_{12}^{(1)}\left(r_1^{\text{meas}},\theta_1^{\text{meas}},\phi_1^{\text{meas}};\omega\right)}{\det\left[\Psi^{(1)}(r,\theta,\phi;\omega)\right]}$$
$$=\frac{2\sqrt{\pi}k\left(r_2^{\text{meas}}\right)^2\left(kr_1^{\text{meas}}+i\right)\cos\theta_1^{\text{meas}}\mathrm{e}^{-ikr_2^{\text{meas}}}}{r_2^{\text{meas}}\left(1-ikr_1^{\text{meas}}\right)\cos\theta_1^{\text{meas}}-r_1^{\text{meas}}\left(1-ikr_2^{\text{meas}}\right)\cos\theta_2^{\text{meas}}},$$

$$-\frac{\Psi_{21}^{(1)}\left(r_2^{\text{meas}},\theta_2^{\text{meas}},\phi_2^{\text{meas}};\omega\right)}{\det\left[\Psi^{(1)}(r,\theta,\phi;\omega)\right]}$$
$$=i2\sqrt{\frac{\pi}{3}}\frac{k^2\left(r_1^{\text{meas}}\right)^2r_2^{\text{meas}}\mathrm{e}^{-ikr_1^{\text{meas}}}}{r_2^{\text{meas}}\left(1-ikr_1^{\text{meas}}\right)\cos\theta_1^{\text{meas}}-r_1^{\text{meas}}\left(1-ikr_2^{\text{meas}}\right)\cos\theta_2^{\text{meas}}},$$

$$\frac{\Psi_{11}^{(1)}\left(r_1^{\text{meas}},\theta_1^{\text{meas}},\phi_1^{\text{meas}};\omega\right)}{\det\left[\Psi^{(1)}(r,\theta,\phi;\omega)\right]}$$
$$=-i2\sqrt{\frac{\pi}{3}}\frac{k^2r_1^{\text{meas}}\left(r_2^{\text{meas}}\right)^2\mathrm{e}^{-ikr_2^{\text{meas}}}}{r_2^{\text{meas}}\left(1-ikr_1^{\text{meas}}\right)\cos\theta_1^{\text{meas}}-r_1^{\text{meas}}\left(1-ikr_2^{\text{meas}}\right)\cos\theta_2^{\text{meas}}}.$$

Accordingly, the reconstructed acoustic pressures are given by

$$\begin{Bmatrix}\hat{p}\left(r_1^{\text{rec}},\theta_1^{\text{rec}},\phi_1^{\text{rec}};\omega\right)\\ \hat{p}\left(r_2^{\text{rec}},\theta_2^{\text{rec}},\phi_2^{\text{rec}};\omega\right)\end{Bmatrix}=-k\begin{bmatrix} i\dfrac{\mathrm{e}^{ikr_1^{\text{rec}}}}{kr_1^{\text{rec}}} & \dfrac{\sqrt{3}\left(kr_1^{\text{rec}}+i\right)\cos\theta_1^{\text{rec}}}{\left(kr_1^{\text{meas}}\right)^2}\mathrm{e}^{ikr_1^{\text{rec}}}\\ i\dfrac{\mathrm{e}^{ikr_2^{\text{rec}}}}{kr_2^{\text{rec}}} & \dfrac{\sqrt{3}\left(kr_2^{\text{rec}}+i\right)\cos\theta_2^{\text{rec}}}{\left(kr_2^{\text{rec}}\right)^2}\mathrm{e}^{ikr_2^{\text{rec}}}\end{bmatrix}$$
$$\times\begin{bmatrix} -\dfrac{\left(r_1^{\text{meas}}\right)^2\left(kr_2^{\text{meas}}+i\right)\cos\theta_2^{\text{meas}}\mathrm{e}^{-ikr_1^{\text{meas}}}}{\Delta} & \dfrac{\left(r_2^{\text{meas}}\right)^2\left(kr_2^{\text{meas}}+i\right)\cos\theta_2^{\text{meas}}\mathrm{e}^{-ikr_2^{\text{meas}}}}{\Delta}\\ i\dfrac{\left(kr_2^{\text{meas}}\right)\left(r_1^{\text{meas}}\right)^2\mathrm{e}^{-ikr_1^{\text{meas}}}}{\sqrt{3}\Delta} & -i\dfrac{\left(kr_1^{\text{meas}}\right)\left(r_2^{\text{meas}}\right)^2\mathrm{e}^{-ikr_2^{\text{meas}}}}{\sqrt{3}\Delta}\end{bmatrix}$$
$$\begin{Bmatrix}\hat{p}\left(r_1^{\text{meas}},\theta_1^{\text{meas}},\phi_1^{\text{meas}};\omega\right)\\ \hat{p}\left(r_2^{\text{meas}},\theta_2^{\text{meas}},\phi_2^{\text{meas}};\omega\right)\end{Bmatrix},$$

where $\Delta=r_2^{\text{meas}}(1-ikr_1^{\text{meas}})\cos\theta_1^{\text{meas}}-r_1^{\text{meas}}(1-ikr_2^{\text{meas}})\cos\theta_2^{\text{meas}}$.

These results are of generality because we have neither specified the measurement points $(r_m^{\text{meas}},\theta_m^{\text{meas}},\phi_m^{\text{meas}};\omega)$, $m=1$ and 2, and the reconstruction points, $(r_s^{\text{rec}},\theta_s^{\text{rec}},\phi_s^{\text{rec}};\omega)$, $m=1$ and 2, nor stipulated the measured acoustic pressures $\hat{p}\left(r_m^{\text{meas}},\theta_m^{\text{meas}},\phi_m^{\text{meas}};\omega\right)$. In practice, however, it will be a good idea to take measurements on a conformal surface very close to the target source surfaces so as to capture as much near-field information as possible.

Once the acoustic pressure is reconstructed, the particle velocity anywhere in the field can be obtained by using the Euler's equation,

$$\vec{\hat{v}}\left(r^{\text{rec}},\theta^{\text{rec}},\phi^{\text{rec}};\omega\right)=\frac{1}{i\omega\rho_0}\nabla\hat{p}\left(r^{\text{rec}},\theta^{\text{rec}},\phi^{\text{rec}};\omega\right).$$

The time-averaged acoustic intensity anywhere in the field is given by

$$\vec{I}_{av}(r^{\text{rec}},\theta^{\text{rec}},\phi^{\text{rec}};\omega)=\frac{1}{2}\text{Re}\left[\hat{p}\left(r^{\text{rec}},\theta^{\text{rec}},\phi^{\text{rec}};\omega\right)\vec{\hat{v}}^{*}\left(r^{\text{rec}},\theta^{\text{rec}},\phi^{\text{rec}};\omega\right)\right].$$

Therefore, all acoustic quantities in the entire field including the source surface are completely determined.

Example 3.2 Now let us specify the input data $\left\{\hat{p}\left(r_m^{\text{meas}},\theta_m^{\text{meas}},\phi_m^{\text{meas}};\omega\right)\right\}_{M\times 1}$. First, we consider the dilating sphere of radius $r=a$ at a constant frequency f. Suppose that the normal surface velocity on this dilating sphere is $\hat{v}_{\text{n}}$. Then acoustic pressure at any arbitrary field point is given by

$$\hat{p}\left(r_m^{\text{meas}},\theta_m^{\text{meas}},\phi_m^{\text{meas}};\omega\right)=\frac{\rho_0 c\hat{v}_{\text{n}}ka^2\text{e}^{ik\left(r_m^{\text{meas}}-a\right)}}{(ka+i)r_m^{\text{meas}}},\quad m=\ 1\text{ and }2.$$

Substituting these data into the expansion coefficients given in Example 3.1 yields

$$\left\{\begin{matrix}C_1(\omega)\\C_2(\omega)\end{matrix}\right\}=2\sqrt{\pi}k\left[\begin{matrix}-\dfrac{\left(r_1^{\text{meas}}\right)^2\left(kr_2^{\text{meas}}+i\right)\cos\theta_2\text{e}^{-ikr_1^{\text{meas}}}}{\Delta} & \dfrac{\left(r_2^{\text{meas}}\right)^2\left(kr_1^{\text{meas}}+i\right)\cos\theta_1\text{e}^{-ikr_2^{\text{meas}}}}{\Delta}\\ i\dfrac{\left(kr_2^{\text{meas}}\right)\left(r_1^{\text{meas}}\right)^2\text{e}^{-ikr_1^{\text{meas}}}}{\sqrt{3}\Delta} & -i\dfrac{\left(kr_1^{\text{meas}}\right)\left(r_2^{\text{meas}}\right)^2\text{e}^{-ikr_2^{\text{meas}}}}{\sqrt{3}\Delta}\end{matrix}\right]$$

$$\times\left\{\begin{matrix}\rho_0 c\hat{v}_{\text{n}}\dfrac{(ka)}{(ka+i)}\left(\dfrac{a}{r_1^{\text{meas}}}\right)\text{e}^{ik\left(r_1^{\text{meas}}-a\right)}\\ \rho_0 c\hat{v}_{\text{n}}\dfrac{(ka)}{(ka+i)}\left(\dfrac{a}{r_2^{\text{meas}}}\right)\text{e}^{ik\left(r_2^{\text{meas}}-a\right)}\end{matrix}\right\}=\left\{\begin{matrix}i2\sqrt{\pi}\rho_0 c\hat{v}_{\text{n}}\dfrac{(ka)^2}{(ka+i)}\text{e}^{-ika}\\ 0\end{matrix}\right\},$$

where Δ is given in Example 3.1.

Once the expansion coefficients are determined, the acoustic pressure anywhere including the source surface can be reconstructed by using the HELS formulation (3.1).

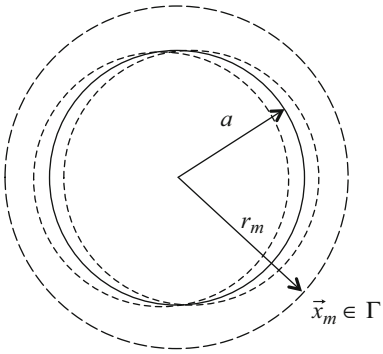

Fig. 3.2 Schematic of reconstructing the acoustic field generated by an oscillating sphere of radius $r = a$ using HELS-based NAH. The measured acoustic pressures are taken on a concentric spherical surface of radius r_m

$$\hat{p}\left(r^{\text{rec}}, \theta^{\text{rec}}, \phi^{\text{rec}}; \omega\right) = \left\{ -i\frac{1}{2\sqrt{\pi}}\frac{\mathrm{e}^{ikr^{\text{rec}}}}{kr^{\text{rec}}} - \frac{1}{2}\sqrt{\frac{3}{\pi}}\frac{\left(kr^{\text{rec}}+i\right)\cos\theta^{\text{rec}}}{\left(kr^{\text{rec}}\right)^2}\mathrm{e}^{ikr^{\text{rec}}} \right\} \left\{ \begin{array}{c} i2\sqrt{\pi}\rho_0 c\hat{v}_{\text{n}}\dfrac{(ka)^2}{(ka+i)}\mathrm{e}^{-ika} \\ 0 \end{array} \right\}$$
$$= \rho_0 c\hat{v}_{\text{n}}\left(\frac{ka}{ka+i}\right)\left(\frac{a}{r^{rec}}\right)\mathrm{e}^{ik\left(r^{\text{rec}}-a\right)},$$

which matches perfectly the analytic solution [42].

Example 3.3 Next, we reconstruct the acoustic pressure generated by a sphere of radius $r = a$ that oscillates in the z-axis direction at a constant frequency f (see Fig. 3.2). Suppose that the normal surface velocity of this oscillating sphere is $\hat{v}_c \cos\theta$. The acoustic pressures at any field point can be written as

$$\hat{p}\left(r_m^{\text{meas}}, \theta_m^{\text{meas}}, \phi_m^{\text{meas}}; \omega\right) = \frac{\rho_0 c\hat{v}_z a^2\left(kr_m^{\text{meas}}+i\right)\cos\theta_m^{\text{meas}}\mathrm{e}^{ik\left(r_m^{\text{meas}}-a\right)}}{\left(k^2a^2-2+i2ka\right)\left(r_m^{\text{meas}}\right)^2}$$
$$= \frac{C_0 a^2\left(kr_m^{\text{meas}}+i\right)\cos\theta_m^{\text{meas}}\mathrm{e}^{ikr_m^{\text{meas}}}}{\left(r_m^{\text{meas}}\right)^2},$$

where $m = 1$ and 2, and the constant C_0 is given by

$$C_0 = \rho_0 c\hat{v}_z\left(\frac{ka}{k^2a^2-2+i2ka}\right)\mathrm{e}^{-ika}.$$

Accordingly, the expansion coefficients are given by

$$\begin{Bmatrix} C_1(\omega) \\ C_2(\omega) \end{Bmatrix}$$

$$= 2\sqrt{\pi}k \begin{bmatrix} -\dfrac{\left(r_1^{\text{meas}}\right)^2\left(kr_2^{\text{meas}}+i\right)\cos\theta_2^{\text{meas}}e^{-ikr_1^{\text{meas}}}}{\Delta} & \dfrac{\left(r_2^{\text{meas}}\right)^2\left(kr_1^{\text{meas}}+i\right)\cos\theta_1^{\text{meas}}e^{-ikr_2^{\text{meas}}}}{\Delta} \\ i\dfrac{\left(kr_2^{\text{meas}}\right)\left(r_1^{\text{meas}}\right)^2\mathrm{e}^{-ikr_1^{\text{meas}}}}{\sqrt{3}\Delta} & -i\dfrac{\left(kr_1^{\text{meas}}\right)\left(r_2^{\text{meas}}\right)^2\mathrm{e}^{-ikr_2^{\text{meas}}}}{\sqrt{3}\Delta} \end{bmatrix},$$

$$\times \begin{Bmatrix} \dfrac{C_0a^2\left(kr_1^{\text{meas}}+i\right)\cos\theta_1^{\text{meas}}\mathrm{e}^{ikr_1^{meas}}}{\left(r_1^{\text{meas}}\right)^2} \\ \dfrac{C_0a^2\left(kr_2^{\text{meas}}+i\right)\cos\theta_2^{\text{meas}}\mathrm{e}^{ikr_2^{\text{meas}}}}{\left(r_2^{\text{meas}}\right)^2} \end{Bmatrix} = \begin{Bmatrix} 0 \\ C_0(ka)^2 \\ -2\sqrt{\dfrac{\pi}{3}} \end{Bmatrix}$$

where Δ is given in Example 3.1.

Using Eq. (3.1), the acoustic pressure anywhere including the source surface is given by

$$\begin{aligned} &\hat{p}\left(r^{\text{rec}},\theta^{\text{rec}},\phi^{\text{rec}};\omega\right) \\ &= -\frac{1}{2\sqrt{\pi}}\begin{Bmatrix} i\mathrm{e}^{ikr^{\text{rec}}} & \dfrac{\sqrt{3}(kr^{\text{rec}}+i)\cos\theta^{\text{rec}}}{\left(kr^{\text{rec}}\right)^2}\mathrm{e}^{ikr^{\text{rec}}} \\ \dfrac{kr^{\text{rec}}}{} & \end{Bmatrix}\begin{Bmatrix} 0 \\ -2\sqrt{\dfrac{\pi}{3}}C_0(ka)^2 \end{Bmatrix}, \\ &= \rho_0c\hat{v}_z\frac{(ka)(kr^{\text{rec}}+i)\cos\theta}{\left(k^2a^2-2+i2ka\right)}\left(\frac{a}{r^{\text{rec}}}\right)^2\mathrm{e}^{ik(r^{\text{rec}}-a)} \end{aligned}$$

which once again agrees perfectly with the analytic solution [42].

3.3 Predicting the Radiated Acoustic Field

In Examples 3.1–3.3 we have focused on using the HELS formulations to reconstruct the acoustic pressure radiated from a vibrating sphere. Now we demonstrate that the same formulations can be used to predict acoustic radiation from a vibrating object.

To this end, we take the normal derivative of Eq. (3.1), and apply the Euler's equation to express the expansion coefficients $\{C\}_{J\times1}$ in terms of the normal surface velocity:

$$i\omega\rho_0\left\{\hat{v}_{\text{n}}\left(\vec{x}_s;\omega\right)\right\}_{S\times1} = \left[\frac{\partial\Psi^{(1)}\left(\vec{x}_s;\omega\right)}{\partial\text{n}}\right]_{S\times J}\{C(\omega)\}_{J\times1}, \tag{3.21}$$

where $\hat{v}_{\mathrm{n}}\left(\vec{x}_s;\omega\right)$ is the normal component of the particle velocity measured by the source surface at $\vec{x}_s$, $s=1, 2, \ldots, S$, and $\{C\}_{J\times 1}$ are obtained by taking a pseudo inversion of Eq. (3.21).

$$\{C(\omega)\}_{J\times 1} = i\omega\rho_0 \left[\frac{\partial \Psi^{(1)}\left(\vec{x}_s;\omega\right)}{\partial \mathrm{n}}\right]^{\dagger}_{J\times S} \left\{\hat{v}_{\mathrm{n}}\left(\vec{x}_s;\omega\right)\right\}_{S\times 1}, \tag{3.22}$$

where the pseudo inversion in Eq. (3.22) is defined as

$$\left[\frac{\partial \Psi^{(1)}\left(\vec{x}_s;\omega\right)}{\partial \mathrm{n}}\right]^{\dagger}_{J\times S} = \left(\left[\frac{\partial \Psi^{(1)}\left(\vec{x}_s;\omega\right)}{\partial \mathrm{n}}\right]^{H}_{J\times S} \left[\frac{\partial \Psi^{(1)}\left(\vec{x}_s;\omega\right)}{\partial \mathrm{n}}\right]_{S\times J}\right)^{-1} \left[\frac{\partial \Psi^{(1)}\left(\vec{x}_s;\omega\right)}{\partial \mathrm{n}}\right]^{H}_{J\times S}, \tag{3.23}$$

where a superscript H implies a Hermitian transpose of a matrix.

Substituting Eq. (3.23) into (3.1) leads to the matrix formulation for predicting acoustic radiation from any vibrating structure into three-dimensional space,

$$\left\{\hat{p}\left(\vec{x};\omega\right)\right\}_{N\times 1} = \left[G_{vp}\left(\vec{x}\middle|\vec{x}_s;\omega\right)\right]_{N\times S} \left\{\hat{v}_{\mathrm{n}}\left(\vec{x}_s;\omega\right)\right\}_{S\times 1}, \tag{3.24}$$

where $\left[G_{vp}\left(\vec{x}\middle|\vec{x}_s;\omega\right)\right]_{N\times S}$ indicates the transfer function that correlates the normal surface velocity specified on the source surface to the field acoustic pressure, which is given by

$$\left[G_{vp}\left(\vec{x}\middle|\vec{x}_s;\omega\right)\right]_{N\times S} = i\omega\rho_0 \left[\Psi^{(1)}\left(\vec{x};\omega\right)\right]_{N\times J} \left[\frac{\partial \Psi^{(1)}\left(\vec{x}_s;\omega\right)}{\partial \mathrm{n}}\right]^{\dagger}_{J\times S}. \tag{3.25}$$

Equation (3.24) can be utilized to predict the acoustic pressure, given the normal surface velocity on a vibrating object.

Let us consider the case that involves two expansion functions such that Eq. (3.24) may be solved exactly. Moreover, the normal surface velocity is specified at two points on the surface of a vibrating sphere of radius $r=a$ at a constant frequency f, and the acoustic pressures at two arbitrary field points are sought. This scenario leads to a square matrix equation given by

$$\begin{Bmatrix} \hat{p}(r_1,\theta_1,\phi_1;\omega) \\ \hat{p}(r_2,\theta_2,\phi_2;\omega) \end{Bmatrix} = i\omega\rho_0 \begin{bmatrix} \Psi_{11}^{(1)}(r_1,\theta_1,\phi_1;\omega) & \Psi_{12}^{(1)}(r_1,\theta_1,\phi_1;\omega) \\ \Psi_{21}^{(1)}(r_2,\theta_2,\phi_2;\omega) & \Psi_{22}^{(1)}(r_2,\theta_2,\phi_2;\omega) \end{bmatrix}$$

$$\times \begin{bmatrix} +\left.\frac{\partial\Psi_{22}^{(1)}\left(r,\theta_2^{\text{meas}},\phi_2^{\text{meas}};\omega\right)}{\partial r}\right|_{r=a} & -\left.\frac{\partial\Psi_{12}^{(1)}\left(r,\theta_1^{\text{meas}},\phi_1^{\text{meas}};\omega\right)}{\partial r}\right|_{r=a} \\ -\left.\frac{\partial\Psi_{21}^{(1)}\left(r,\theta_2^{\text{meas}},\phi_2^{\text{meas}};\omega\right)}{\partial r}\right|_{r=a} & +\left.\frac{\partial\Psi_{11}^{(1)}\left(r,\theta_1^{\text{meas}},\phi_1^{\text{meas}};\omega\right)}{\partial r}\right|_{r=a} \end{bmatrix} \frac{\begin{Bmatrix} \hat{v}_{\text{n}}\left(a,\theta_1^{\text{meas}},\phi_1^{\text{meas}};\omega\right) \\ \hat{v}_{\text{n}}\left(a,\theta_2^{\text{meas}},\phi_2^{\text{meas}};\omega\right) \end{Bmatrix}}{\det\left[\left.\frac{\partial\Psi^{(1)}(r,\theta,\phi;\omega)}{\partial r}\right|_{r=a}\right]}, \tag{3.26}$$

where the determinant is given by

$$\begin{aligned} \det\left[\left.\frac{\partial\Psi^{(1)}(r,\theta,\phi;\omega)}{\partial r}\right|_{r=a}\right] = {} & \left.\frac{\partial\Psi_{11}^{(1)}\left(r,\theta_1^{\text{meas}},\phi_1^{\text{meas}};\omega\right)}{\partial r}\right|_{r=a} \left.\frac{\partial\Psi_{22}^{(1)}\left(r,\theta_2^{\text{meas}},\phi_2^{\text{meas}};\omega\right)}{\partial r}\right|_{r=a} \\ & - \left.\frac{\partial\Psi_{21}^{(1)}\left(r,\theta_1^{\text{meas}},\phi_1^{\text{meas}};\omega\right)}{\partial r}\right|_{r=a} \left.\frac{\partial\Psi_{12}^{(1)}\left(r,\theta_2^{\text{meas}},\phi_2^{\text{meas}};\omega\right)}{\partial r}\right|_{r=a}, \end{aligned} \tag{3.27}$$

where the first subscript in the expansion functions implies the order of expansion functions, and the second subscript stands for the sequence of measurement points. The expansion functions and their derivatives are given by

$$\Psi_{11}^{(1)}(r_1,\theta_1,\phi_1;\omega) = -i\frac{1}{2\sqrt{\pi}}\frac{\mathrm{e}^{ikr_1}}{kr_1}, \tag{3.28}$$

$$\Psi_{12}^{(1)}(r_1,\theta_1,\phi_1;\omega) = -\frac{1}{2}\sqrt{\frac{3}{\pi}}\frac{(kr_1+i)\mathrm{e}^{ikr_1}}{k^2r_1^2}\cos\theta_1, \tag{3.29}$$

$$\Psi_{21}^{(1)}(r_2,\theta_2,\phi_2;\omega) = -i\frac{1}{2\sqrt{\pi}}\frac{\mathrm{e}^{ikr_2}}{kr_2}, \tag{3.30}$$

$$\Psi_{22}^{(1)}(r_2,\theta_2,\phi_2;\omega) = -\frac{1}{2}\sqrt{\frac{3}{\pi}}\frac{(kr_2+i)\mathrm{e}^{ikr_2}}{k^2r_2^2}\cos\theta_2 \tag{3.31}$$

$$\left.\frac{\partial\Psi_{11}^{(1)}\left(r,\theta_1^{\text{meas}},\phi_1^{\text{meas}};\omega\right)}{\partial r}\right|_{r=a} = \frac{1}{2\sqrt{\pi}}\frac{(ka+i)\mathrm{e}^{ika}}{ka^2}, \tag{3.32}$$

$$\left.\frac{\partial\Psi_{12}^{(1)}\left(r,\theta_1^{\text{meas}},\phi_1^{\text{meas}};\omega\right)}{\partial r}\right|_{r=a} = \frac{1}{2}\sqrt{\frac{3}{\pi}}\frac{\left[2ka+i\left(2-k^2a^2\right)\right]\mathrm{e}^{ika}}{k^2a^3}\cos\theta_1^{\text{meas}}, \tag{3.33}$$

$$\left.\frac{\partial \Psi_{22}^{(1)}\left(r,\theta_2^{\text{meas}},\phi_2^{\text{meas}};\omega\right)}{\partial r}\right|_{r=a} = \frac{1}{2\sqrt{\pi}}\frac{(ka+i)\mathrm{e}^{ika}}{ka^2}, \tag{3.34}$$

$$\left.\frac{\partial \Psi_{22}^{(1)}\left(r,\theta_2^{\text{meas}},\phi_2^{\text{meas}};\omega\right)}{\partial r}\right|_{r=a} = \frac{1}{2}\sqrt{\frac{3}{\pi}}\frac{\left[2ka+i\left(2-k^2a^2\right)\right]\mathrm{e}^{ika}}{k^2a^3}\cos\theta_2^{\text{meas}}, \tag{3.35}$$

where θ_m^{meas}, $m=1$ and 2, indicates the polar angles at the measurement points on the sphere.

Substituting the expansion functions and their derivatives into the determinant yields

$$\begin{aligned}&\det\left[\left.\frac{\partial \Psi^{(1)}(r,\theta,\phi;\omega)}{\partial r}\right|_{r=a}\right]\\ &=\frac{\sqrt{3}}{4\pi}\frac{(ka+i)\left[2ka+i\left(2-k^2a^2\right)\right]\mathrm{e}^{i2ka}}{k^3a^5}\left(\cos\theta_2^{\text{meas}}-\cos\theta_1^{\text{meas}}\right).\end{aligned} \tag{3.36}$$

Substituting Eqs. (3.28)–(3.35) and (3.36) into (3.26), we obtain

$$\begin{aligned}\begin{Bmatrix}\hat{p}\left(r_1,\theta_1,\phi_1;\omega\right)\\ \hat{p}\left(r_2,\theta_2,\phi_2;\omega\right)\end{Bmatrix} &= i\omega\rho_0\begin{bmatrix}-i\dfrac{\mathrm{e}^{ikr_1}}{kr_1} & -\sqrt{3}\dfrac{(kr_1+i)\mathrm{e}^{ikr_1}}{k^2r_1^2}\cos\theta_1\\ -i\dfrac{\mathrm{e}^{ikr_2}}{kr_2} & -\sqrt{3}\dfrac{(kr_2+i)\mathrm{e}^{ikr_2}}{k^2r_2^2}\cos\theta_2\end{bmatrix}\\ &\times\begin{bmatrix}\dfrac{ka^2\mathrm{e}^{-ika}}{(ka+i)}\left(\dfrac{\cos\theta_2^{\text{meas}}}{\cos\theta_2^{\text{meas}}-\cos\theta_1^{\text{meas}}}\right) & -\dfrac{ka^2\mathrm{e}^{-ika}}{(ka+i)}\left(\dfrac{\cos\theta_1^{\text{meas}}}{\cos\theta_2^{\text{meas}}-\cos\theta_1^{\text{meas}}}\right)\\ -\dfrac{k^2a^3\mathrm{e}^{-ika}}{\left[2ka+i\left(2-k^2a^2\right)\right]\left(\cos\theta_2^{\text{meas}}-\cos\theta_1^{\text{meas}}\right)} & \dfrac{k^2a^3\mathrm{e}^{-ika}}{\left[2ka+i\left(2-k^2a^2\right)\right]\left(\cos\theta_2^{\text{meas}}-\cos\theta_1^{\text{meas}}\right)}\end{bmatrix}\\ &\times\begin{Bmatrix}\hat{v}_{\text{n}}\left(a,\theta_1^{\text{meas}},\phi_1^{\text{meas}};\omega\right)\\ \hat{v}_{\text{n}}\left(a,\theta_2^{\text{meas}},\phi_2^{\text{meas}};\omega\right)\end{Bmatrix},\end{aligned} \tag{3.37}$$

Equation (3.37) is of generality for a spherical source surface because neither the normal surface velocity nor the measurement and field points are specified.

Example 3.4 Consider the case of a dilating sphere for which the normal surface velocity $\hat{v}_{\text{n}}$ is a constant (see Fig. 3.3). Substituting $\hat{v}_{\text{n}}$ into Eq. (3.37), we obtain

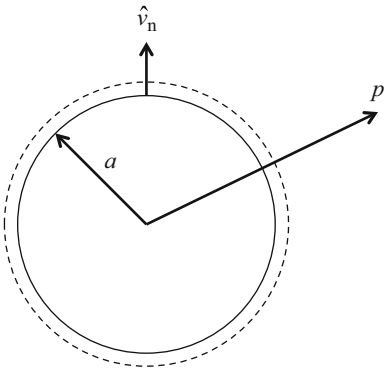

Fig. 3.3 Schematic of predicting the acoustic field generated by a dilating sphere of radius $r = a$ by using HELS-based NAH. The normal surface velocity is given at two arbitrary points on the surface and the field acoustic pressure is predicted

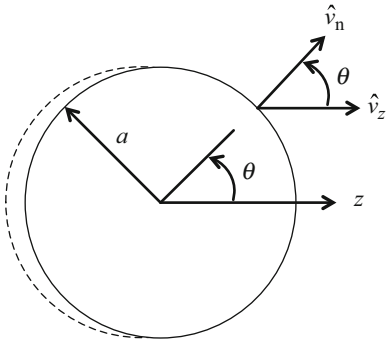

Fig. 3.4 Schematic of predicting the acoustic field generated by a sphere of radius a oscillating along the z-axis direction by using HELS-based NAH. The normal surface velocity is specified at two arbitrary points on the surface and the field acoustic pressure is predicted

$$\left\{ \begin{array}{l} \hat{p}\left(r_1, \theta_1, \phi_1; \omega\right) \\ \hat{p}\left(r_2, \theta_2, \phi_2; \omega\right) \end{array} \right\} = \left[\begin{array}{ll} -i\dfrac{\mathrm{e}^{ikr_1}}{kr_1} & -\sqrt{3}\dfrac{(kr_1+i)\mathrm{e}^{ikr_1}}{k^2 r_1^2}\cos\theta_1 \\ -i\dfrac{\mathrm{e}^{ikr_2}}{kr_2} & -\sqrt{3}\dfrac{(kr_2+i)\mathrm{e}^{ikr_2}}{k^2 r_2^2}\cos\theta_2 \end{array} \right]$$

$$\left\{ i\rho_0 c\hat{v}_{\mathrm{n}} \frac{(ka)^2}{(ka+i)} \mathrm{e}^{-ika} 0 \right\} = \left\{ \begin{array}{l} \rho_0 c\hat{v}_{\mathrm{n}} \left(\dfrac{ka}{ka+i}\right)\left(\dfrac{a}{r_1}\right)\mathrm{e}^{ik(r_1-a)} \\ \rho_0 c\hat{v}_{\mathrm{n}} \left(\dfrac{ka}{ka+i}\right)\left(\dfrac{a}{r_2}\right)\mathrm{e}^{ik(r_2-a)} \end{array} \right\},$$

which is exactly the same as the analytic solution [42].

Example 3.5 Next, we consider a sphere of radius $r = a$ that oscillates back and forth in the z-axis direction at the velocity $\hat{v}_z$ (see Fig. 3.4). The normal surface

velocity measured at two arbitrary points on the surface can be written as $\hat{v}_{\mathrm{n}}(a,\theta,\phi;\omega)=\hat{v}_z\cos\theta_m^{\mathrm{meas}}$, $m=1$ and 2,

$$\begin{Bmatrix}\hat{p}\,(r_1,\theta_1,\phi_1;\omega)\\ \hat{p}\,(r_2,\theta_2,\phi_2;\omega)\end{Bmatrix}=\begin{bmatrix}\dfrac{\mathrm{e}^{ikr_1}}{\sqrt{3}kr_1} & -\dfrac{i(kr_1+i)\mathrm{e}^{ikr_1}}{k^2r_1^2}\cos\theta_1\\ \dfrac{\mathrm{e}^{ikr_2}}{\sqrt{3}kr_2} & -\dfrac{i(kr_2+i)E^{ikr_2}}{k^2r_2^2}\cos\theta_2\end{bmatrix}$$
$$\begin{Bmatrix}0\\ \rho_0c\hat{v}_z\dfrac{(ka)^3}{2ka+i\left(2-k^2a^2\right)}\mathrm{e}^{-ika}\end{Bmatrix}$$
$$=\begin{Bmatrix}\rho_0c\hat{v}_z\dfrac{(ka)(kr_1+i)E^{ik(r_1-a)}}{\left(k^2a^2-2\right)+i2ka}\left(\dfrac{a}{r_1}\right)^2\cos\theta_1\\ \rho_0c\hat{v}_z\dfrac{(ka)(kr_2+i)\mathrm{e}^{ik(r_2-a)}}{\left(k^2a^2-2\right)+i2ka}\left(\dfrac{a}{r_2}\right)^2\cos\theta_2\end{Bmatrix},$$

which again matches the analytic solution perfectly [42].

3.4 Error Analyses

To acquire an in-depth understanding of the HELS solutions (3.16) and (3.18), we carry out an error analysis to see the impact of the measurement errors on reconstruction results.

There are different types of errors in the measured data that can be caused by a number of reasons due to aliasing, aperture size, bias, random fluctuations, etc. Most of these errors may be corrected by using various techniques that have been developed in the past. For example, temporal and spatial aliasing can be overcome by using sufficiently high sampling rates in either temporal or spatial special domains; errors due to a finite measurement aperture can be reduced by applying a spatial window to the measured data; biased errors can be adjusted by calibrating the system, and random fluctuations can be suppressed by taking time averages of the measurements. In this error analysis, however, we do not distinguish the causes of errors. Moreover, we assume that they are uncorrelated to the true values of the measured data. Accordingly, Eq. (3.16) can be written as

$$\left\{\hat{p}\left(\vec{x}_S^{\,\mathrm{rec}};\omega\right)\right\}_{S\times1}=\left[G_{pp}\left(\vec{x}_S^{\,\mathrm{rec}}\middle|\vec{x}_m^{\,\mathrm{meas}};\omega\right)\right]_{S\times M}^{-1}\left\{\hat{p}\left(\vec{x}_m^{\,\mathrm{meas}};\omega\right)+\varepsilon_m\right\}_{M\times1},\tag{3.38}$$

where ε_m represents the measurement errors that are Gaussian white and spatially uncorrelated.

As an example, we consider the two-term expansion ($n=1$) and assume that the acoustic pressure is specified on a spherical surface of radius $r=r_m$, $m=1$ and 2. Substituting the expansion functions $\Psi_{ij}^{(1)}(r_i,\theta_i,\phi_i;\omega)$ into Eq. (3.38) yields the following explicit solutions:

$$\begin{Bmatrix} \hat{p}\left(r_1^{\mathrm{rec}},\theta_1^{\mathrm{rec}},\phi_1^{\mathrm{rec}};\omega\right) \\ \hat{p}\left(r_2^{\mathrm{rec}},\theta_2^{\mathrm{rec}},\phi_2^{\mathrm{rec}};\omega\right) \end{Bmatrix} = \begin{Bmatrix} G_{11}\hat{p}\left(r_1^{\mathrm{meas}},\theta_1^{\mathrm{meas}},\phi_1^{\mathrm{meas}};\omega\right) - G_{12}\hat{p}\left(r_2^{\mathrm{meas}},\theta_2^{\mathrm{meas}},\phi_2^{\mathrm{meas}};\omega\right) + O_1(\varepsilon_1,\varepsilon_2) \\ G_{21}\hat{p}\left(r_1^{\mathrm{meas}},\theta_1^{\mathrm{meas}},\phi_1^{\mathrm{meas}};\omega\right) - G_{22}\hat{p}\left(r_2^{\mathrm{meas}},\theta_2^{\mathrm{meas}},\phi_2^{\mathrm{meas}};\omega\right) + O_2(\varepsilon_1,\varepsilon_2) \end{Bmatrix}, \tag{3.39}$$

where G_{ij} are defined as

$$G_{11} = \frac{\Psi_{11}^{(1)}\left(r_1^{\mathrm{rec}},\theta_1^{\mathrm{rec}},\phi_1^{\mathrm{rec}};\omega\right)\Psi_{22}^{(1)}\left(r_2^{\mathrm{meas}},\theta_2^{\mathrm{meas}},\phi_2^{\mathrm{meas}};\omega\right) - \Psi_{12}^{(1)}\left(r_1^{\mathrm{rec}},\theta_1^{\mathrm{rec}},\phi_1^{\mathrm{rec}};\omega\right)\Psi_{21}^{(1)}\left(r_2^{\mathrm{meas}},\theta_2^{\mathrm{meas}},\phi_2^{\mathrm{meas}};\omega\right)}{\det\left[\Psi^{(1)}(r^{\mathrm{meas}},\theta^{\mathrm{meas}},\phi^{\mathrm{meas}};\omega)\right]}, \tag{3.40}$$

$$G_{12} = \frac{\Psi_{11}^{(1)}\left(r_1^{\mathrm{rec}},\theta_1^{\mathrm{rec}},\phi_1^{\mathrm{rec}};\omega\right)\Psi_{12}^{(1)}\left(r_1^{\mathrm{meas}},\theta_1^{\mathrm{meas}},\phi_1^{\mathrm{meas}};\omega\right) - \Psi_{12}^{(1)}\left(r_1^{\mathrm{rec}},\theta_1^{\mathrm{rec}},\phi_1^{\mathrm{rec}};\omega\right)\Psi_{11}^{(1)}\left(r_1^{\mathrm{meas}},\theta_1^{\mathrm{meas}},\phi_1^{\mathrm{meas}};\omega\right)}{\det\left[\Psi^{(1)}(r^{\mathrm{meas}},\theta^{\mathrm{meas}},\phi^{\mathrm{meas}};\omega)\right]}, \tag{3.41}$$

$$G_{21} = \frac{\Psi_{21}^{(1)}\left(r_2^{\mathrm{rec}},\theta_2^{\mathrm{rec}},\phi_2^{\mathrm{rec}};\omega\right)\Psi_{22}^{(1)}\left(r_2^{\mathrm{meas}},\theta_2^{\mathrm{meas}},\phi_2^{\mathrm{meas}};\omega\right) - \Psi_{22}^{(1)}\left(r_2^{\mathrm{rec}},\theta_2^{\mathrm{rec}},\phi_2^{\mathrm{rec}};\omega\right)\Psi_{21}^{(1)}\left(r_2^{\mathrm{meas}},\theta_2^{\mathrm{meas}},\phi_2^{\mathrm{meas}};\omega\right)}{\det\left[\Psi^{(1)}(r^{\mathrm{meas}},\theta^{\mathrm{meas}},\phi^{\mathrm{meas}};\omega)\right]}, \tag{3.42}$$

$$G_{22} = \frac{\Psi_{21}^{(1)}\left(r_2^{\mathrm{rec}},\theta_2^{\mathrm{rec}},\phi_2^{\mathrm{rec}};\omega\right)\Psi_{12}^{(1)}\left(r_1^{\mathrm{meas}},\theta_1^{\mathrm{meas}},\phi_1^{\mathrm{meas}};\omega\right) - \Psi_{22}^{(1)}\left(r_2^{\mathrm{rec}},\theta_2^{\mathrm{rec}},\phi_2^{\mathrm{rec}};\omega\right)\Psi_{11}^{(1)}\left(r_1^{meas},\theta_1^{\mathrm{meas}},\phi_1^{\mathrm{meas}};\omega\right)}{\det\left[\Psi^{(1)}(r^{\mathrm{meas}},\theta^{\mathrm{meas}},\phi^{\mathrm{meas}};\omega)\right]}, \tag{3.43}$$

where the determinant is given by

$$\begin{aligned}&\det\left[\Psi^{(1)}(r^{\text{meas}},\theta^{\text{meas}},\phi^{\text{meas}};\omega)\right]\\&\quad=\Psi_{11}^{(1)}\left(r_1^{\text{meas}},\theta_1^{\text{meas}},\phi_1^{\text{meas}};\omega\right)\Psi_{22}^{(1)}\left(r_2^{\text{meas}},\theta_2^{\text{meas}},\phi_2^{\text{meas}};\omega\right)\\&\qquad-\Psi_{12}^{(1)}\left(r_1^{\text{meas}},\theta_1^{\text{meas}},\phi_1^{\text{meas}};\omega\right)\Psi_{21}^{(1)}\left(r_2^{\text{meas}},\theta_2^{\text{meas}},\phi_2^{\text{meas}};\omega\right).\end{aligned}\tag{3.44}$$

The error terms in Eq. (3.39) are defined as

$$\left\{\begin{array}{l}O_1(\varepsilon_1,\varepsilon_2)\\O_2(\varepsilon_1,\varepsilon_2)\end{array}\right\}=\left\{\begin{array}{l}G_{11}\varepsilon_1-G_{12}\varepsilon_2\\G_{21}\varepsilon_1-G_{22}\varepsilon_2\end{array}\right\},\tag{3.45}$$

where G_{ij} are given in Eq. (3.40)–(3.43).

Equation (3.39) has generality for a spherical source since neither the measured acoustic pressures $\hat{p}\left(r_m^{\text{meas}},\theta_m^{\text{meas}},\phi_m^{\text{meas}};\omega\right)$ nor the measurement points $(r_m,\theta_m,\phi_m;\omega)$, $m=1$ and 2, as well as the reconstruction points $(r_s^{\text{rec}},\theta_s^{\text{rec}},\phi_s^{\text{rec}};\omega)$, $s=1$ and 2, are specified.

Substituting the expressions for individual expansion functions $\Psi_{ij}^{(1)}$ as given in Example 3.1 to Eq. (3.40-3.43) and further to Eq. (3.45), we can write the leading order terms of errors as

$$\left\{\begin{array}{l}O_1(\varepsilon_1,\varepsilon_2)\\O_2(\varepsilon_1,\varepsilon_2)\end{array}\right\}=\left\{\begin{array}{l}a_1\left(\frac{r_1^{\text{meas}}}{r_1^{\text{rec}}}\right)^2\varepsilon_1+a_2\left(\frac{r_2^{\text{meas}}}{r_1^{\text{rec}}}\right)^2\varepsilon_2\\b_1\left(\frac{r_1^{\text{meas}}}{r_2^{\text{rec}}}\right)^2\varepsilon_1+b_2\left(\frac{r_2^{\text{meas}}}{r_2^{\text{rec}}}\right)^2\varepsilon_2\end{array}\right\},\tag{3.46}$$

where a_m and b_m, $m=1$ and 2, are independent of the radial distance r. Equation (3.46) show that when $r_s^{\text{rec}}<r_m^{\text{meas}}$, the measurement errors ε_m can be amplified quadratically.

It is easy to show that if we consider a single-term expansion, namely, $n=0$ in (3.38), the error term will be proportional to $(r_m^{\text{meas}}/r_s^{\text{rec}})$, where $r_s^{\text{rec}}<r_m^{\text{meas}}$,

$$O(\varepsilon)=a\left(\frac{r^{\text{meas}}}{r^{\text{rec}}}\right)\varepsilon,\tag{3.47}$$

where a is independent of the radial distance.

These results can be extended to any order of expansion in $\Psi_{ij}^{(1)}$. As shown in Example 2.2, the asymptotic behaviors of the spherical Hankel function of the first kind as $kr\to 0$, namely, the reconstruction point approaches the source surface, are given by

$$h_n^{(1)}(kr)\to\frac{1}{(kr)^{n+1}}.\tag{3.48}$$

So for the nth-order expansion of $\Psi_{ij}^{(1)}$ in Eq. (3.38), the reconstruction errors are dominated by

$$O_s(\varepsilon_1, \varepsilon_2, \ldots, \varepsilon_M) = \sum_{m=1}^{M} a_m \left(\frac{r_m^{\text{meas}}}{r_s^{\text{rec}}} \right)^{n+1} \varepsilon_m, \quad r_s^{\text{rec}} < r_m^{\text{meas}} \tag{3.49}$$

where a_m, $m = 1, 2, \ldots, M$, are independent of the radial distance. Since $r_s^{\text{rec}} < r_m^{\text{meas}}$, $(r_m^{\text{meas}}/r_s^{\text{rec}}) > 1$. Therefore, the measurement errors ε_m are amplified by $(r_m^{\text{meas}}/r_s^{\text{rec}})^{n+1}$ times in reconstruction.

Equation (3.49) demonstrates the importance of keeping the measurement surface close to the source surface in order to ensure the accuracy in reconstruction.

However, when the HELS formulations (3.24) are utilized to predict the radiated acoustic pressure, given the normal surface velocity of a vibrating structure, errors in the predicted results will be bounded.

Following the procedures outlined above, it can be shown that the errors in Eq. (3.24) are proportional to

$$O(\varepsilon) \propto \sum_{n=0}^{N} \sum_{m=1}^{M} \frac{h_n^{(1)}(kr^{\text{rec}})}{dh_n^{(1)}\left(kr_m^{\text{meas}}\right)/d\left(kr_m^{\text{meas}}\right)} \varepsilon_m. \tag{3.50}$$

Example 2.3 illustrates that the asymptotic behaviors of the spherical Hankel functions and their derivatives in the far-field ($kr \to \infty$) are given by

$$h_n^{(1)}(kr) \to \frac{1}{kr} \text{and} \frac{dh_n^{(1)}(kr)}{d(kr)} \to \frac{1}{kr}. \tag{3.51}$$

Substituting Eq. (3.51) into (3.50) yields the upper bound of the errors $O(\varepsilon)$ in Eq. (3.24),

$$O(\varepsilon) \propto N \sum_{m=1}^{M} b_m \left(\frac{r_m^{\text{meas}}}{r^{\text{rec}}} \right) \mathrm{e}^{ikr^{\text{rec}}} \varepsilon_m \le N \sum_{m=1}^{M} b_m \left(\frac{r_m^{\text{meas}}}{r^{\text{rec}}} \right) |\varepsilon_m|, \tag{3.52}$$

where N represents the total number of the spherical Hankel functions involved in the expansion, and b_m, $m = 1$ and 2, are independent of the radial distance.

Since $r^{\text{meas}} < r^{\text{rec}}$, $(r_m^{\text{meas}}/r_s^{\text{rec}}) < 1$. So the errors in prediction are always bounded. In fact, the further the prediction distance r^{rec} is, the smaller the errors in prediction become.

As the field point r^{rec} approaches the source surface ($kr \to 0$), the asymptotic behaviors of the spherical Hankel functions and their derivatives are given by (see Example 2.2),

$$h_n^{(1)}(kr) \to \frac{1}{(kr)^{n+1}} \text{and} \frac{dh_n^{(1)}(kr)}{d(kr)} \to \frac{1}{(kr)^{n+2}}. \tag{3.53}$$

Substituting Eq. (3.53) into (3.50) leads to the errors $O(\varepsilon)$ in Eq. (3.24),

$$O(\varepsilon) \propto \sum_{n=0}^{N} \sum_{m=1}^{M} b_m\left(kr_m^{\text{meas}}\right)\left(\frac{r_m^{\text{meas}}}{r^{\text{rec}}}\right)^{n+1} \varepsilon_m. \tag{3.54}$$

Since $(r_m^{\text{meas}}/r_s^{\text{rec}}) < 1$, the errors in prediction using Eq. (3.24) are bounded by

$$O(\varepsilon) \leq \sum_{m=1}^{M} b_m\left(kr_m^{\text{meas}}\right)\left(\frac{r_m^{\text{meas}}}{r^{\text{rec}}}\right)|\varepsilon_m|. \tag{3.55}$$

Therefore, errors in measurements ε_m will not affect the acoustic pressure in prediction as much as they do in reconstruction.

3.5 Regularization

The examples discussed in Sects. 3.2–3.4 all dealt with a spherical source surface. In practice, a vibrating structure is seldom spherical. Moreover, the measured acoustic pressures are neither accurate nor complete. So the acoustic quantities reconstructed by using Eqs. (3.15) and (3.17) may be quite unsatisfactory. This is because reconstruction is an inverse process, namely, we want to identify the cause (e.g., structural vibrations) based on the effect (the resultant acoustic pressure field). Such a problem is mathematically ill posed. Accordingly, any slight error in the input data may be amplified significantly as it has been demonstrated in the preceding error analysis section.

The solution strategies to an inverse problem encountered in all fields can be summarized in one word: regularization [43]. The underlying principle in all regularization techniques is to smooth the dependence of the output data on the input data [44–46].

The simplest regularization for Eq. (3.15) is to use an optimal number of expansion terms J_{op} in reconstruction. This is because Eq. (3.15) employs the superposition of the spherical wave functions to describe the acoustic pressure. The more expansion terms are used in Eq. (3.15), the more details in the reconstructed acoustic pressure are included. Theoretically, if the input data are accurate and complete, the expansion solution given by Eq. (3.15) for a spherical source is exact as $J \to \infty$ [47]. However, this is not the case in reality. Sect. 3.4 has shown that errors embedded in measurement ε_m can be amplified by $(r_m^{\text{meas}}/r_s^{\text{rec}})^{n+1}$ times in reconstruction on the source surface. Therefore, it is necessary to find the optimal number of expansion J_{op} in reconstruction.

In what follows, we consider an arbitrarily shaped source surface and the measured data are neither accurate nor complete. For convenience sake, we express the basis functions in terms the spherical Hankel functions and spherical harmonics since they are available in many mathematical libraries. Use of these spherical wave functions may be very effective for a surface with an aspect ratio close to unity, $x: y: z \to 1$. For elongated, flat, or both elongated and flat objects, the prolate,

oblate, or elliptic coordinates, respectively, can be used to provide faster convergence in numerical computations. Unfortunately, the analytic forms of the spheroidal functions in these corresponding coordinates are nonexistent and direct numerical computations of these spheroidal functions must be carried out, which can be extremely time consuming.

3.6 Regularization Through Truncation of the Expansion Functions

In this section, we want to develop a simple yet effective methodology to reconstruct the radiated acoustic pressure field. To achieve this goal, we must devise a procedure that can yield the desired accuracy with relatively few measurements. The questions that must be addressed are:

1. Where and how the measurements should be taken?
2. How many measurement points are necessary to achieve the desired resolution?
3. Given the number of measurements, what is the optimal number of expansion functions?

Unfortunately, there are no definite answers to these questions because of the uncertainties involved in an inverse problem. What we can do is to develop guidelines with which satisfactory reconstruction of the radiated acoustic pressure fields can be obtained. The detailed guidelines are presented in Chap. 5.

Suppose that the input data are collected by an array of microphones (see Fig. 3.5). For simplicity yet without loss of generality, we use a rectangular array that consists of $M_1 \times M_2 = M$ microphones and collect M data points.

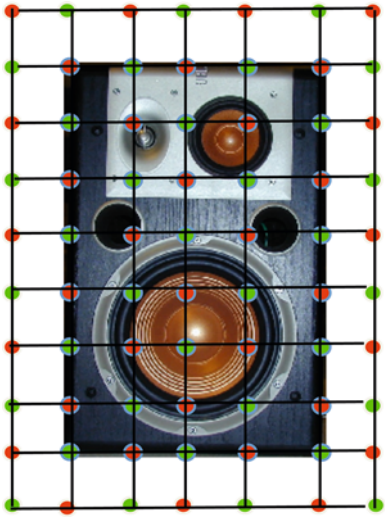

Fig. 3.5 An array of $M_1 \times M_2$ microphones used to reconstruct the acoustic pressures radiated from a source. *Red dots*, input data points; *green dots,* validation points

These measured data can be substituted into Eq. (3.15) to reconstruct the acoustic pressure anywhere.

To find an optimal number of expansion terms in reconstruction, we only use one-half the data points and the other half for validation. Detailed procedures are as follows:

1. Use every other data points (red dots) as indicated in Fig. 3.5 as input to Eq. (3.15) to reconstruct the acoustic pressures at other points on the hologram surface (green dots) with $N=1$ and $J=(N+1)^2=4$ terms for any selected frequency f. The corresponding expansion functions include $h_0(kr_m)P_{0,0}(\cos\theta_m)$, $h_1(kr_m)P_{1,0}(\cos\theta_m)$, $h_1(kr_m)P_{1,1}(\cos\theta_m)\sin\phi_m$, and $h_1(kr_m)P_{1,1}(\cos\theta_m)\cos\phi_m$.
2. Calculate the L2-norm errors of the reconstructed acoustic pressures at the green dots with respect to the measured data.

$$\|L\|^2=\sum_{m=1}^{M/2}\left|\hat{p}^{\,\mathrm{rec}}(r_m,\theta_m,\phi_m;\omega)-\hat{p}^{\,\mathrm{meas}}(r_m,\theta_m,\phi_m;\omega)\right|^2, \tag{3.56}$$

   where $m=1$ to $M/2$.

3. Increase the number of expansion terms by one, $J=J+1$ in Eq. (3.15) and repeat the same processes as outlined in 1 and 2 and calculate the L2-norm errors again.
4. Find the minimum value of L2-norm errors. Notice that because of uncertainties involved in the measurements, L2-norm errors may fluctuate with respect to the value of J. However the general trend of this L2-norm error curve is U-shaped. Accordingly, its slope becomes zero at the global minimum of the L2-norm error curve, and the corresponding value of J is optimal. The resultant expansions will provide the best approximation of the reconstructed acoustic pressure on the source surface. In practice, an exact zero slope may not occur. So we can set a criterion for the slope to be less than certain value, say, $\tan\alpha\le\varepsilon_0$, where ε_0 is a preselected small value. The corresponding number of expansion terms is the optimal value J_{op}, which can be interpreted as being optimized with respect to a particular set of the measured acoustic pressures at a particular frequency f. Obviously, different frequency and measurement conditions will yield a different optimal value of J_{op}.

In general, the higher the frequency f is, the larger the value of J_{op} becomes and the longer the computation takes. This slowdown in computation speed is inherent in all expansion theories, including the standard finite element or boundary element methods. Therefore other methods such as asymptotic approximations should be utilized to reconstruct the radiated acoustic pressure field in the high-frequency regime.

The value of J_{op} thus determined may be used to reconstruct acoustic pressures anywhere, including the source surface.

Example 3.6 Figure 3.6 displays a typical example [37] of L2-norm errors curves for reconstructing the acoustic pressures with respect to benchmark values on a

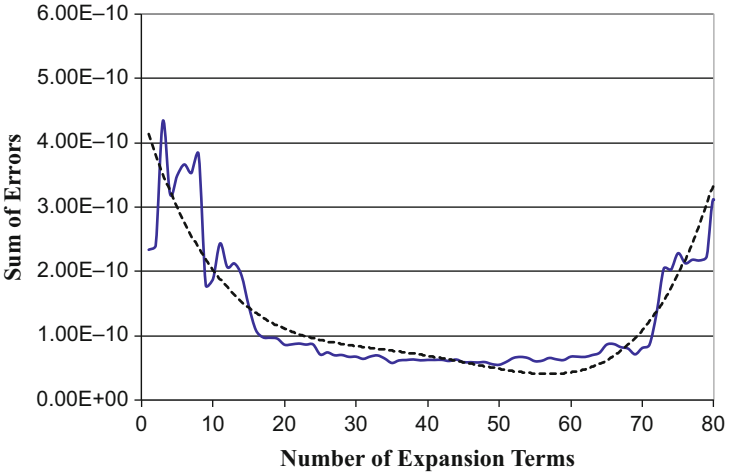

Fig. 3.6 The L2-norm errors curves with respect to the expansion terms for the reconstructed acoustic pressure on a source surface. *Solid line*, errors; *dashed line,* curve-fitted errors

source surface. Results indicate that the accuracy in reconstruction on the source surface increases at first with the number of expansion terms to certain level, and then decreases monotonically thereafter. The presence of this minimum L2-norm error is reasonable. Physically, the higher-order terms represent the small-scale or near-field effects, which may have been lost in the measured data and cannot be recovered anyway. On the other hand, the lower-order terms describe the large-scale or propagating wave effects, which may be captured in the measured data and can be reconstructed. As more expansion functions are used in reconstruction, more details are added to the reconstructed acoustic pressure and therefore, more accurate the result is. However the higher the order of expansions is, the more the amplifications of measurement errors in the reconstructed acoustic pressure become (see Sect. 3.4). Eventually, the errors embedded in the high-order terms will be so large that they may completely distort the reconstructed acoustic pressures.

Consequently, it is necessary to find the optimal number of expansion terms in order to get a satisfactory reconstruction of the radiated acoustic pressure field in both near and far fields in a cost-effective manner in practice.

On the other hand, the L2-norm error curves for the acoustic pressures reconstructed on the measurement surface shows a monotonic decay with respect to the expansion terms. In other words, the accuracy in reconstruction on the measurement surface increases monotonically with the number of expansion terms (Fig. 3.7). This is expected because errors in reconstruction on a measurement surface have been minimized by the least-squares method.

It is emphasized that the above optimization process is effective for producing a satisfactory reconstruction for the acoustic pressure, but not enough for reconstructing the normal component of the particle velocity on a vibrating surface.

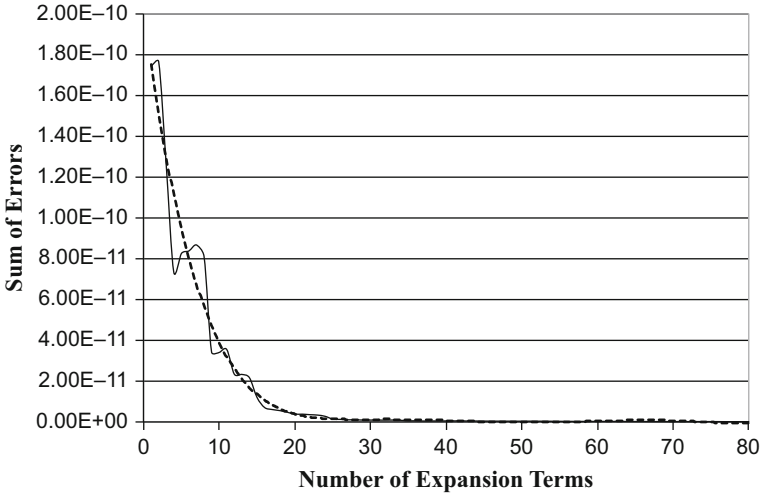

Fig. 3.7 The L2-norm errors curves with respect to the expansion terms for the reconstructed acoustic pressure on a measurement surface. *Solid line*, errors; *dashed line*, curve-fitted errors

This is because the normal surface velocity usually contains much more details (evanescent waves) than the acoustic pressure do. Accordingly, different methods must be used to ensure a satisfactory reconstruction of the normal surface velocity.

3.7 Other Regularization Techniques

Consider Eqs. (3.15) and (3.17), which represent the explicit solutions for the reconstructed surface acoustic pressure and normal surface velocity. Since in practice the measured data will not be error free and the source surface may not be spherical, the transfer matrices on the right sides of Eqs. (3.15) and (3.17), $\left[G_{pp}\left(\vec{x}_s^{\,\mathrm{rec}}\middle|\vec{x}_m^{\,\mathrm{meas}};\omega\right)\right]^{-1}_{S\times M}$ and $\left[G_{pv}\left(\vec{x}_s^{\,\mathrm{rec}}\middle|\vec{x}_m^{\,\mathrm{meas}};\omega\right)\right]^{-1}_{S\times M}$, may be singular and errors embedded in the measured data $\hat{p}\left(\vec{x}_m^{\,\mathrm{meas}};\omega\right)$ may grow without a bound. One way to obtain a bounded solution is to apply a truncated singular value decomposition (TSVD) to Eqs. (3.15) and (3.17) [22]

$$\left\{\hat{p}\left(\vec{x}_s^{\,\mathrm{rec}};\omega\right)\right\}_{S\times 1}=\left[V_p\right]_{S\times S}\left[\sum\nolimits_p\right]^{-1}_{S\times M}\left[U_p\right]^{H}_{M\times M}\left\{\hat{p}\left(\vec{r}_m^{\,\mathrm{meas}};\omega\right)\right\}_{M\times 1}, \quad (3.57)$$

$$\left\{\hat{v}_{\mathrm{n}}\left(\vec{x}_s^{\,\mathrm{rec}};\omega\right)\right\}_{S\times 1}=[V_v]_{S\times S}\left[\sum\nolimits_v\right]^{-1}_{S\times M}[U_v]^H_{M\times M}\left\{\hat{p}\left(\vec{r}_m^{\,\mathrm{meas}};\omega\right)\right\}_{M\times 1}, \tag{3.58}$$

where $[V_p]$ and $[U_p]$ in Eq. (3.57) are the right and left unitary orthonormal matrices, respectively, of the matrix $\left[G_{pp}\left(\vec{x}_s^{\,\mathrm{rec}}\middle|\vec{x}_m^{\,\mathrm{meas}};\omega\right)\right]^{-1}_{S\times M}$ in Eq. (3.15), $[\Sigma_p]^{-1}$ is the diagonal matrix that contains inverted singular values of the corresponding matrix; $[V_v]$ and $[U_v]$ in Eq. (3.58) are the right and left unitary orthonormal matrices, respectively, of the matrix $\left[G_{pv}\left(\vec{x}_s^{\,\mathrm{rec}}\middle|\vec{x}_m^{\,\mathrm{meas}};\omega\right)\right]^{-1}_{S\times M}$ in Eq. (3.17), and $[\Sigma_v]^{-1}$ is the diagonal matrix containing inverted singular values of the corresponding matrix.

The simplest regularization for the HELS method is to set the number of expansion terms in Eqs. (3.57) and (3.58) at the optimal value J_{op} for any given set of the input data, as discussed above. Mathematically, this optimization process can be written as

$$\min_J \sum_{i=1}^{M}\left\|\hat{p}\left(\vec{x}_{m,i}^{\,\mathrm{rec}};\omega\right)-\hat{p}\left(\vec{x}_{m,i}^{\,\mathrm{meas}};\omega\right)\right\|_2^2\rightarrow J_{\mathrm{op}}, \tag{3.59}$$

where $\hat{p}\left(\vec{x}_{m,i}^{\,\mathrm{rec}};\omega\right)$ and $\hat{p}\left(\vec{x}_{m,i}^{\,\mathrm{meas}};\omega\right)$ represent, respectively, the reconstructed and measured acoustic pressures at the ith measurement point $\vec{x}_{m,i}$. As pointed out above, Eq. (3.59) may be effective for reconstructing the acoustic pressure, but not enough for the normal surface velocity.

The effectiveness of using regularization methods such as Tikhonov regularization (TR) and L-curve. to improve the accuracy in reconstruction by HELS has been examined previously [48]. Results have indicated that the modified Tikhonov regularization [49] (MTR) with its regularization parameter determined by the generalized cross-validation [50] (GCV) can provide the most accurate reconstruction for HELS.

Recently, hybrid regularization [51] has been developed to determine the optimal number for the basis functions. In this hybrid regularization the MTR and GCV method are used to regularize the reconstruction of acoustic pressures on a hologram surface for each value of J first, and the least-squares method to minimize residual by matching the reconstructed acoustic pressure with respect to the measured one. Mathematically, this process is expressible as

$$\min_J \sum_{m=1}^{M}\left\|\hat{p}\left(\vec{x}_m^{\,\mathrm{rec},\alpha};\omega\right)-\hat{p}\left(\vec{x}_m^{\,\mathrm{meas}};\omega\right)\right\|_2^2\rightarrow J_{\mathrm{op,MTR}}, \tag{3.60}$$

where $\hat{p}\left(\vec{x}_m^{\,\mathrm{rec},\alpha};\omega\right)$ is the reconstructed acoustic pressure at the ith measurement point $\vec{x}_m$ by using MTR and GCV, and the Tikhonov functional, J_α, for regularizing $\hat{p}\left(\vec{x}_m^{\,\mathrm{rec},\alpha};\omega\right)$ in Eq. (3.60) may be written as

$$\begin{aligned}
&\mathbf{J}_\alpha\left(\left\{\hat{p}\left(\vec{x}_m^{\,\mathrm{rec},\alpha};\omega\right)\right\}_{M\times 1}\right)\\
&=\left\|[U]_{M\times M}[\Sigma]_{M\times M}[V]^H_{M\times M}\left\{\hat{p}\left(\vec{x}_m^{\,\mathrm{rec},\alpha};\omega\right)\right\}_{M\times 1}-\left\{\hat{p}\left(\vec{x}_m^{\,\mathrm{meas}};\omega\right)\right\}_{M\times 1}\right\|_2^2\\
&\quad+\alpha\left\|\left[F_h^\alpha\right]_{M\times M}[V]^H_{M\times M}\left\{\hat{p}\left(\vec{x}_m^{\,\mathrm{rec}};\omega\right)\right\}_{M\times 1}\right\|_2^2,
\end{aligned}\tag{3.61}$$

where the regularization parameter α is determined by GCV through a minimization process,

$$\min_\alpha\left(\frac{\left\|\left[F_h^\alpha\right]_{M\times M}[U]^H_{M\times M}\left\{\hat{p}\left(\vec{x}_m^{\,\mathrm{meas}};\omega\right)\right\}_{M\times 1}\right\|_2^2}{\left(\mathrm{Trace}\left[F_h^\alpha\right]_{M\times M}\right)^2}\right),\tag{3.62}$$

where $[F_h^\alpha]_{M\times M}$ is the high-pass filter defined as

$$\left[F_h^\alpha\right]_{M\times M}=\mathrm{diag}\left([\mathbf{I}]_{M\times M}-[F^\alpha]_{M\times M}\right),\tag{3.63}$$

where $[F^\alpha]_{M\times M}$ is a low-pass filter for regularizing the measured acoustic pressure and is a diagonal matrix containing the singular values σ_i of the matrix $[\Sigma]$ in Eq. (3.61), where $i=1$ to M,

$$[F^\alpha]_{M\times M}=\mathrm{diag}\left(\ldots,\frac{\sigma_i^2\left(\alpha+\sigma_i^2\right)^2}{\alpha^3+\sigma_i^2\left(\alpha+\sigma_i^2\right)^2},\ldots\right).\tag{3.64}$$

The reconstructed acoustic pressure $\left\{\hat{p}\left(\vec{x}_m^{\,\mathrm{rec},\alpha};\omega\right)\right\}_{M\times 1}$ can then be rewritten as

$$\left\{\hat{p}\left(\vec{x}_m^{\,\mathrm{rec},\alpha};\omega\right)\right\}_{M\times 1}=[V]_{M\times M}[F^\alpha]_{M\times M}[\Sigma]^{-1}_{M\times M}[U]^H_{M\times M}\left\{p\left(\vec{x}_m^{\,\mathrm{meas}};\omega\right)\right\}_{M\times 1}.\tag{3.65}$$

The differences between Eq. (3.15) and Eq. (3.65) are that the former relies on the least-squares method to determine the optimal HELS expansion number J_{op} to reconstruct the acoustic pressure, whereas the latter uses a hybrid regularization that consists of MTR, SVD, and the least-squares minimization to determine the optimal HELS expansion number $J_{\mathrm{op,MTR}}$ and to reconstruct the acoustic pressure.

Using $J_{\mathrm{op,MTR}}$, the acoustic quantities anywhere can be reconstructed. For example, we can express the reconstructed surface acoustic pressure and normal surface velocity as

$$\left\{\hat{p}\left(\vec{x}_s^{\,\mathrm{rec},\alpha};\omega\right)\right\}_{S\times 1} = [V_p]_{S\times S}\left[F_p^{\beta}\right]_{S\times S}[\Sigma_p]^{-1}_{S\times M}[U_p]^{H}_{M\times M}\left\{p\left(\vec{x}_m^{\,\mathrm{meas}};\omega\right)\right\}_{M\times 1}, \tag{3.66}$$

$$\left\{\hat{v}_{\mathrm{n}}\left(\vec{x}_s^{\,\mathrm{rec},\alpha};\omega\right)\right\}_{S\times 1} = [V_v]_{S\times S}\left[F_v^{\gamma}\right]_{S\times S}\left[\sum\nolimits_v\right]^{-1}_{S\times M}[U_v]^{H}_{M\times M}\left\{\hat{p}\left(\vec{x}_m^{\,\mathrm{meas}};\omega\right)\right\}_{M\times 1}, \tag{3.67}$$

where $[F_p^{\beta}]$ and $[F_v^{\gamma}]$ are the diagonal matrices containing the singular values of the matrix $[\Sigma_p]$ in Eq. (3.66) and those of $[\Sigma_v]$ in Eq. (3.67), respectively,

$$\left[F_p^{\beta}\right]_{S\times S} = \mathrm{diag}\left(\ldots, \frac{\varepsilon_i^2\left(\beta+\varepsilon_i^2\right)^2}{\beta^3+\varepsilon_i^2\left(\beta+\varepsilon_i^2\right)^2}, \ldots\right), \tag{3.68}$$

$$\left[F_v^{\gamma}\right]_{S\times S} = \mathrm{diag}\left(\ldots, \frac{\eta_i^2\left(\gamma+\eta_i^2\right)^2}{\gamma^3+\eta_i^2\left(\gamma+\eta_i^2\right)^2}, \ldots\right), \tag{3.69}$$

where β and γ are obtained by GCV through a minimization process given by, respectively,

$$\min_{\beta}\left(\frac{\left\|\left[F_{h,p}^{\beta}\right]_{M\times M}[U_p]^{H}_{M\times M}\left\{\hat{p}\left(\vec{x}_m^{\,\mathrm{meas}};\omega\right)\right\}_{M\times 1}\right\|_2^2}{\left(\mathrm{Trace}\left[F_{h,p}^{\beta}\right]_{M\times M}\right)^2}\right), \tag{3.70}$$

$$\min_{\gamma}\left(\frac{\left\|\left[F_{h,p}^{\gamma}\right]_{M\times M}[U_v]^{H}_{M\times M}\left\{\hat{p}\left(\vec{x}_m^{\,\mathrm{meas}};\omega\right)\right\}_{M\times 1}\right\|_2^2}{\left(\mathrm{Trace}\left[F_{h,p}^{\gamma}\right]_{M\times M}\right)^2}\right), \tag{3.71}$$

where $[F_{h,p}^{\beta}]$ and $[F_{h,v}^{\gamma}]$ are the high-pass filters obtained by subtracting the low-pass filters $[F_p^{\beta}]$ and $[F_v^{\gamma}]$ from the identity matrix, respectively, and by filling its null space with unity,

$$\left[F_{p,h}^{\beta}\right]_{M\times M} = \mathrm{diag}\left[\left([\mathbf{I}]_{S\times S} - \left[F_p^{\beta}\right]_{S\times S}\right), [\mathbf{I}]_{(M-S)\times(M-S)}\right], \tag{3.72}$$

$$\left[F_{v,h}^{\gamma}\right]_{M\times M} = \mathrm{diag}\left[\left([\mathbf{I}]_{S\times S} - \left[F_v^{\gamma}\right]_{S\times S}\right), [\mathbf{I}]_{(M-S)\times(M-S)}\right]. \tag{3.73}$$

Experimental results have confirmed that Eqs. (3.66) and (3.67) can yield more robust results than Eqs. (3.15) and (3.17) do.

Example 3.7 Consider a thin square plate mounted on a large baffle. The addition of a baffle allows for rigorous examinations of the reconstructed vibro-acoustic quantities with respect to the analytic solutions. Also, a plate represents a class of structures that are commonly encountered in practice, as many structures consist of flat or slightly curved panels. Hence it will have significant impacts if we can show

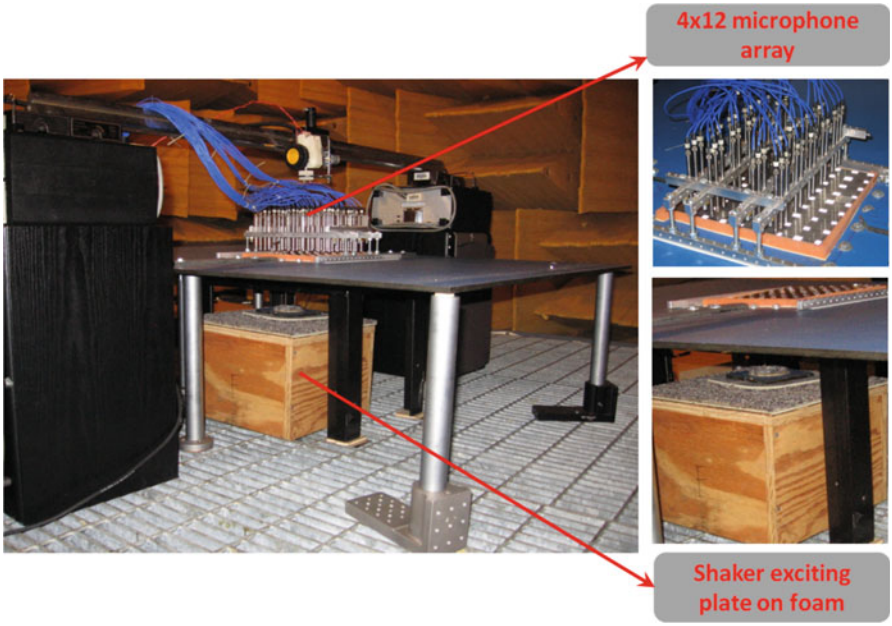

Fig. 3.8 Test setup for collecting the near-field acoustic pressures above a baffled square plate

the capability of using computationally simple HELS codes based on the spherical wave functions to produce satisfactory reconstruction of the vibro-acoustic quantities on a highly non-spherical panel surface.

For convenience yet without loss of generality, we consider a square plate subject to free-free boundary conditions. The reason for choosing a square plate is that its symmetry can pose a challenge for traditional Experimental Modal Analysis (EMA) to distinguish coupled modes. It is interesting to examine if the HELS-based NAH can discern these coupled modes.

Figure 3.8 shows the test setup of a square steel plate of dimensions 220×220 mm^2 with a thickness of 1.25 mm, which was mounted on a large baffle and excited by a mechanical shaker using random signals. The plate edges were supported on soft foam to mimic free-free boundary conditions. The excitation point on the thin plate was selected to be away from the nodal lines of the first 10 natural modes. The radiated acoustic pressures were measured by using a 12×4 array that contained 48 microphones (PCB T130D21, PCB Piezotronics, Inc. Depew, New York). Measurements were taken on three patches, resulting in total 144 data points at the standoff distance of 10 mm.

The tests were conducted inside a fully anechoic chamber at the Acoustics, Vibration, and Noise Control Laboratory at Wayne State University. The excitation signal level was adjusted to ensure that the signal to noise ratio (SNR) was maintained at least 10 dB or higher over the entire frequency of interest. The relative phases of the acoustic pressures were obtained by taking cross correlations of the measured acoustic

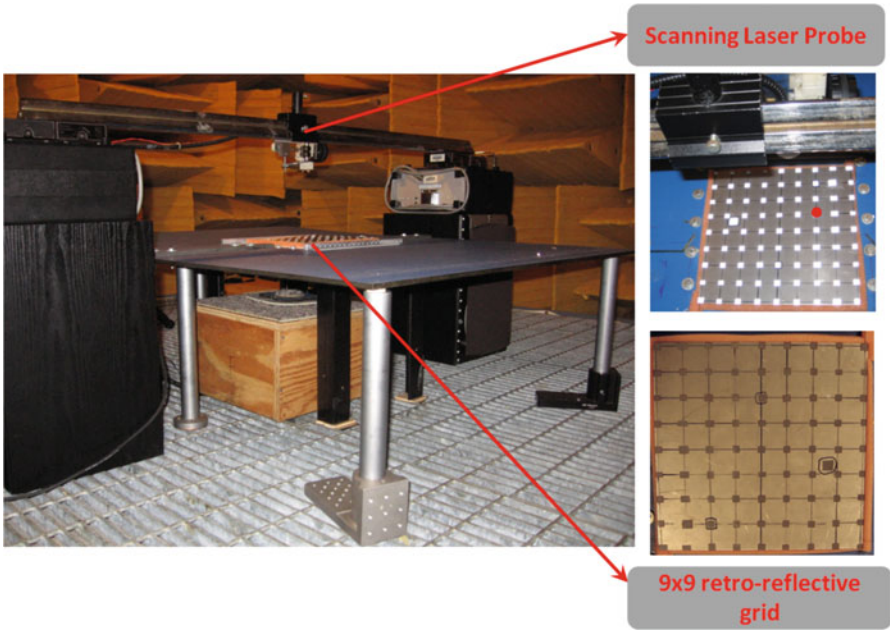

Fig. 3.9 Test setup for reconstructing the vibro-acoustic responses of a baffled square plate using the HELS-based NAH

pressures with respect to the excitation force as a reference signal. The measured data were used as input to the HELS codes to reconstruct the normal surface velocity distributions on the 9×9 grid that coincided with the laser scanning measurement points (see Fig. 3.9). A point laser vibrometer (Polytec OFV 551 fiber optic interferometer, Polytec, Irvine, California) was used to collect the benchmark data to validate the reconstructed normal surface velocity. The measured normal surface velocities were taken as input to EMA to identify the natural modes of the plate.

Figure 3.10 shows the comparison of the acoustic pressures reconstructed at four randomly selected locations on the hologram plane using hybrid regularization with the optimal number of expansion terms $J_{\text{op,MTR}}$ determined by Eq. (3.60). For comparison purposes, we also employed Eq. (3.15) with the optimal number of expansion terms J_{op} given by the least-squares minimization process Eq. (3.59) to reconstruct the acoustic pressures at the same locations. Results confirm that even with a straight application of the HELS method using the value of J_{op}, the accuracy in the reconstructed acoustic pressure is still very high. By using the hybrid regularization strategies, we can get more accurate reconstruction of the acoustic pressures over a much wider frequency span than those obtained by using the least-squares minimization alone.

Figure 3.11 shows the comparison of the minimized residuals in reconstructing the acoustic pressure over the entire frequency range of interest on the hologram surface by using J_{op} and those by using $J_{\text{op,MTR}}$. These results clearly show the advantage of using $J_{\text{op,MTR}}$ in reconstruction.

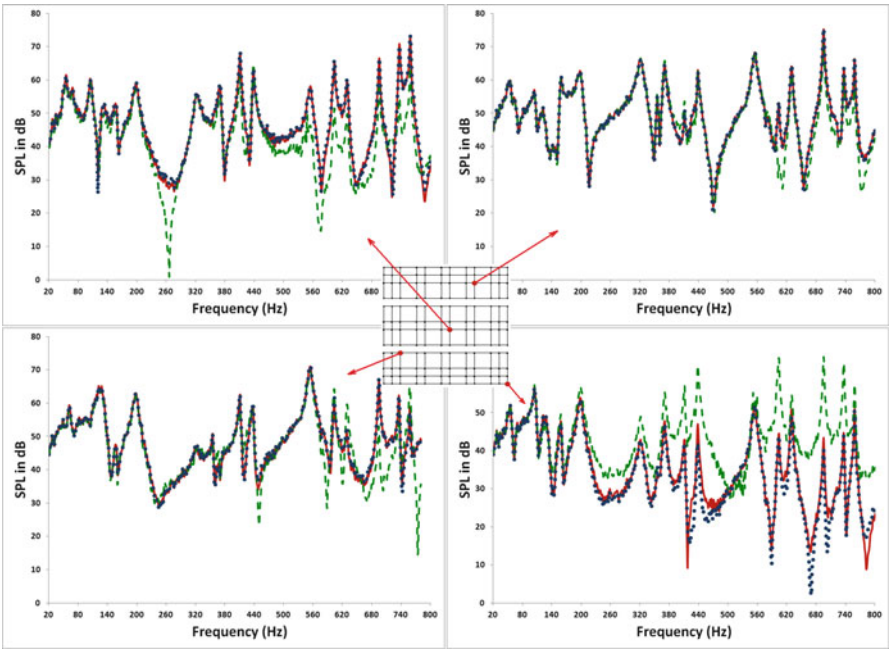

Fig. 3.10 Comparisons of the reconstructed acoustic pressures at four randomly selected points vs. the benchmark results on the hologram surface. *Solid line*, benchmark results; *dotted line*, reconstructed by using the least-squares minimization alone; *crosses*, reconstructed by using the hybrid regularization

Figure 3.12 depicts the comparisons of the normal surface velocity spectra reconstructed at randomly selected points on the plate surface, including its edge and corner, and benchmark data. Once again, we utilized the optimal number of expansion terms J_{op} given by Eq. (3.59) (dashed lines) and that of expansion terms $J_{\text{op},MTR}$ provided by Eq. (3.60) (dotted lines) to reconstruct the normal surface velocities. The results indicate that a straight application of the HELS formulations with J_{op} yields satisfactory reconstruction in the normal surface velocity distributions at the lower-order modes; however, errors in reconstructions increase with the mode order. This is because the number of expansion terms J_{op} obtained by the least-squares minimization alone can be optimal for reconstructing the acoustic pressure, but not enough for reconstructing the normal surface velocity. By using the optimal number of expansion terms $J_{\text{op},MTR}$ obtained through a hybrid regularization scheme, satisfactory reconstruction in the normal surface velocity distribution can be obtained up to the operational deflection shape (ODS) dominated by the natural mode of the target structural wavelength λ_{cr}. The accuracy is improved even along the edges and at corners of the plate.

Figures 3.13 and 3.14 exhibit comparisons of the first 18 natural modes and corresponding natural frequencies of this square plate under free-free boundary conditions from 100 to 420 Hz and from 420 to 800 Hz, respectively.

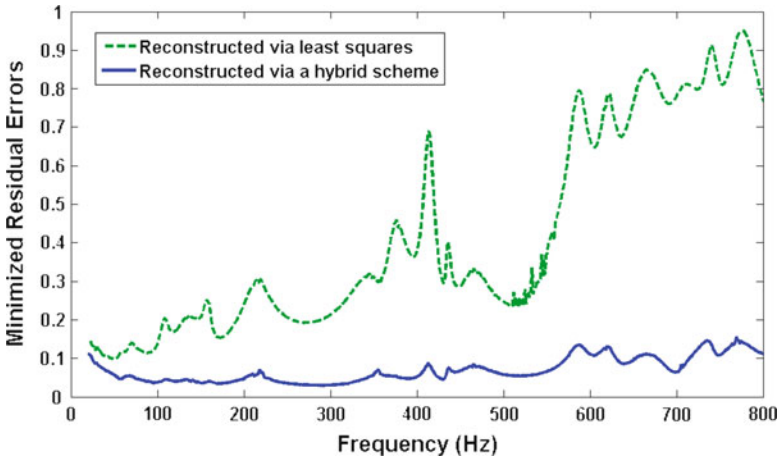

Fig. 3.11 Comparison of the minimized residuals in reconstructing the acoustic pressures by using J_{op} and $J_{\text{op,MTR}}$. *Dashed line,* residuals resulting from $J_{\text{op;}}$ solid line, residuals resulting from $J_{\text{op,MTR}}$

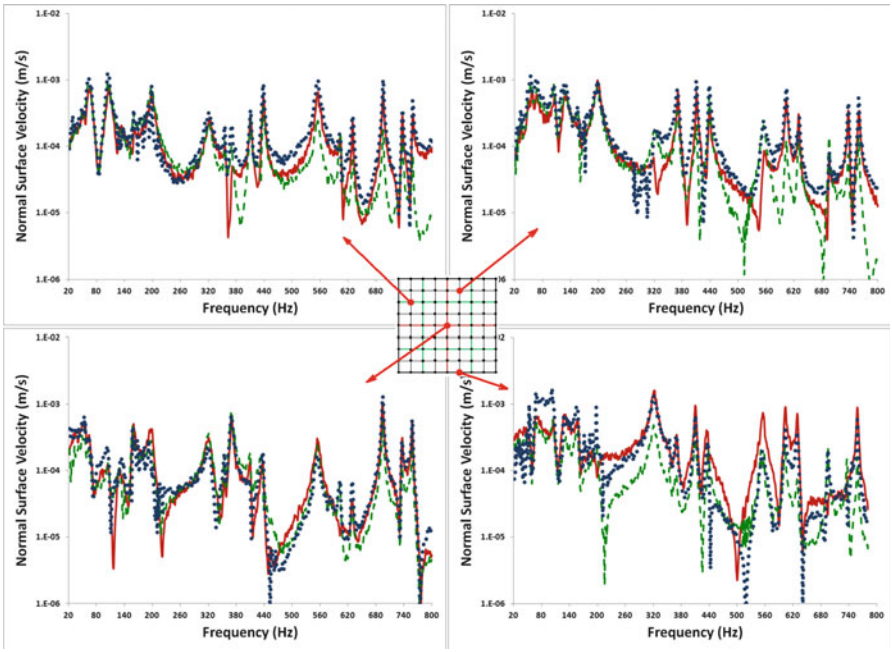

Fig. 3.12 Comparisons of the reconstructed normal surface velocity spectra at some randomly selected points on the baffled square plate surface with the benchmark data. Solid line, benchmark; dotted line, reconstructed using least-squares minimization alone; crosses, reconstructed using a hybrid regularization

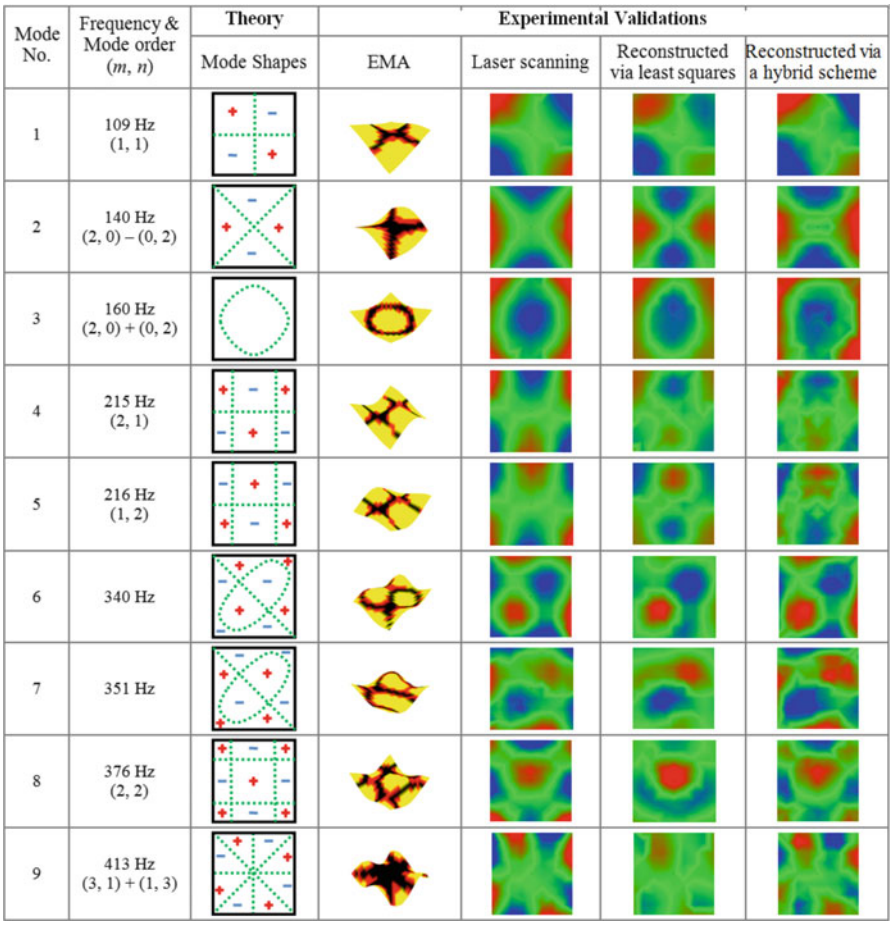

Fig. 3.13 Comparisons of the reconstructed ODS of a baffled square plate subject to free-free boundary conditions and measured ones from 100 to 420 Hz. The first column indicates the mode number, second column implies the mode order and natural frequency, third column shows the theoretical mode shape, fourth column displays the mode shape extracted from EMA, fifth column exhibits the directly measured ODS from laser scanning, and sixth and seventh columns are the reconstructed ODS using the least-squares method and hybrid regularization scheme, respectively

Note that the natural modes extracted by EMA were based on a 9×9 measurement grid, which enabled one to get the 15th mode at 695 Hz successfully. On the other hand, the microphone grid used for HELS reconstruction was based on a 12×12 array, which allowed for a satisfactory reconstruction up to the 18th natural mode. It is emphasized that the theoretical natural modes and those extracted by using EMA were displayed in Figs. 3.13 and 3.14 as a reference, but not for validation. The reconstructed normal surface velocity distributions were validated against the ODS dominated by the 18th natural mode that were obtained by scanning a laser vibrometer on the plate surface. For comparisons beyond the

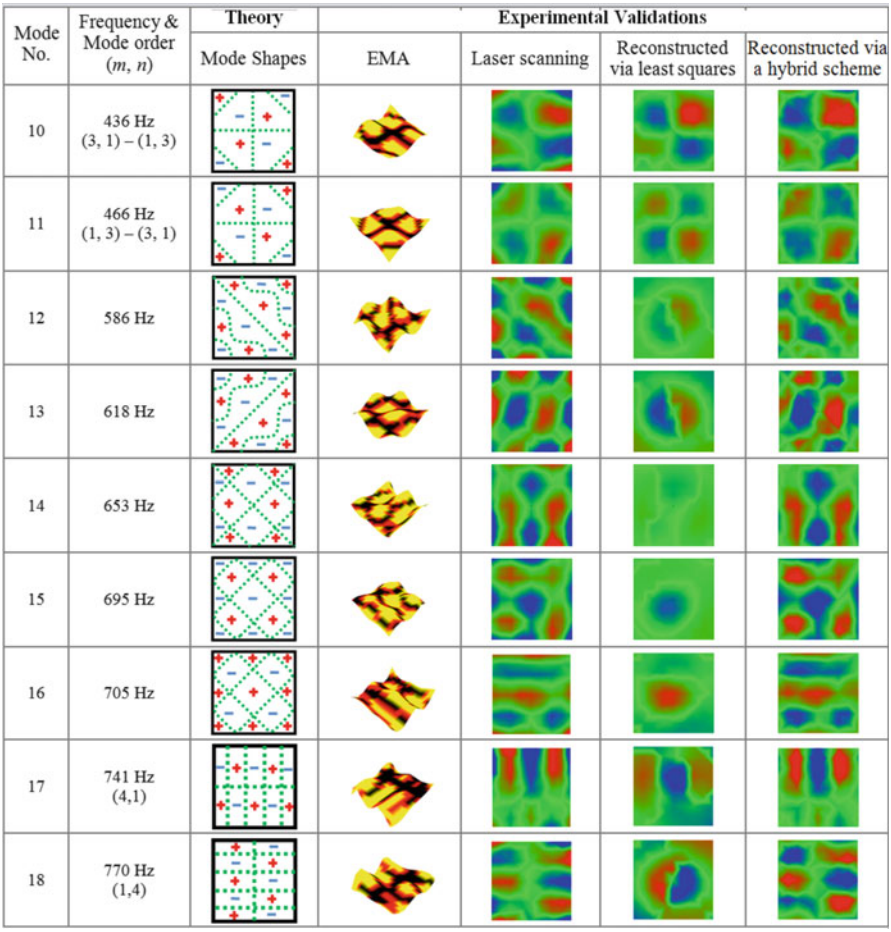

Fig. 3.14 Comparisons of reconstructed ODS of a baffled square plate subject to the free-free boundary condition and measured ones from 420 to 800 Hz. The first column indicates the mode number, second column implies the mode order and natural frequency, third column shows the theoretical mode shape, fourth column displays the mode shape extracted from EMA, fifth column exhibits the directly measured ODS from laser scanning, and sixth and seventh columns are the reconstructed ODS obtained by using the least-squares method alone and by a hybrid regularization scheme, respectively

18th natural mode, a denser measurement grid for the laser vibrometer and a finer measurement grid for the HELS-based NAH must be adopted.

The results shown in Figs. 3.13 and 3.14 confirm that: (1) the HELS based NAH can be utilized to reconstruct the ODSs dominated by the natural modes of a panel structure; (2) a direct application of the HELS formulations using J_{op} alone can yield satisfactory reconstructions of the ODSs dominated by lower-order modes, for example, up to the 11th natural mode in this case; and (3) by using the hybrid regularization scheme, it is possible to obtain satisfactory reconstructions

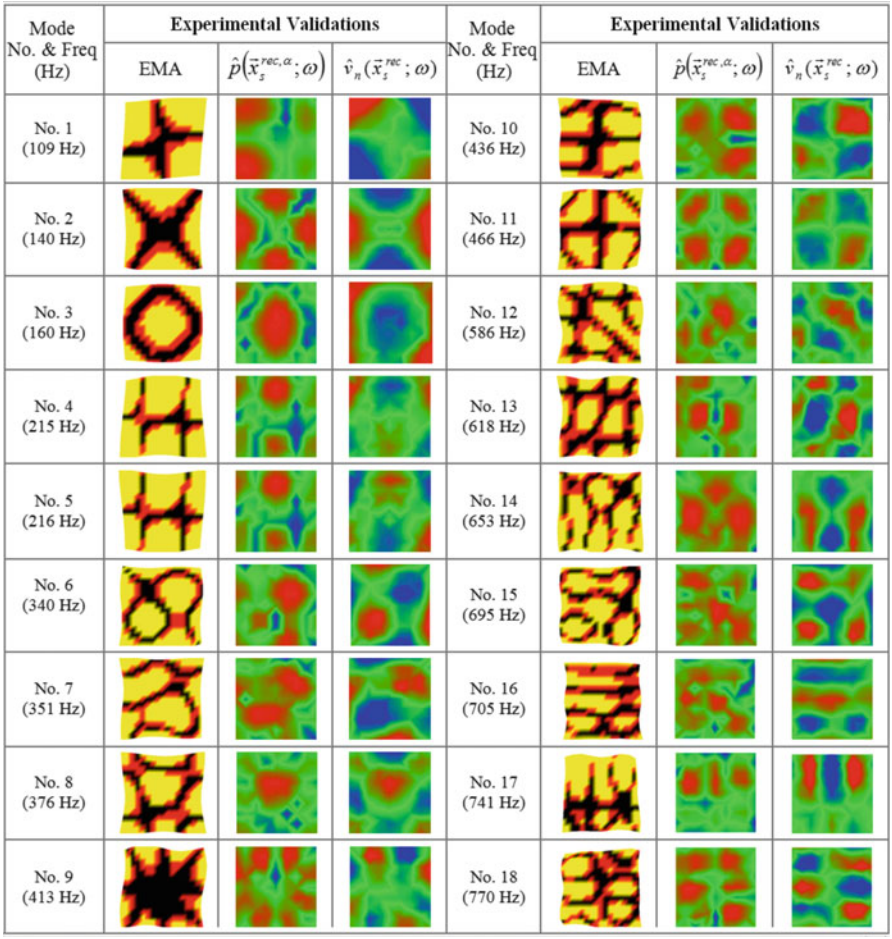

Fig. 3.15 Comparisons of the reconstructed vibro-acoustic quantities on the surface of a baffled square plate up to the 18th natural mode at 770 Hz. The first column is the mode number and frequency; second depicts the mode shape extracted from EMA; third and forth columns demonstrate the surface acoustic pressure and normal surface velocity distributions reconstructed by using the HELS-based NAH with $J_{\text{op,MTR}}$ determined by hybrid regularization scheme, respectively

of all ODSs up to the target one that is dominated by the 18th natural mode of the square plate.

Note that it is not possible to measure the surface acoustic pressure directly. So validations of the reconstructed acoustic pressures are performed on the hologram surface (see Fig. 3.9). It is important, however, to display the capabilities of reconstructing all vibro-acoustic quantities by using the HELS-based NAH at any frequency. Figure 3.15 depicts the natural modes extracted by EMA together with the surface acoustic pressure and normal surface velocity distributions at the natural

frequencies of a square plate up to the 18th natural mode. Note that the acoustic pressure distributions showed the same patterns as those of the normal surface velocity distributions, but without the presence of phase changes. This is because the acoustic pressure is a scalar quantity.

The HELS-based NAH has been successfully used to reconstruct acoustic radiation from arbitrarily shaped objects in both exterior [52, 53] and interior regions [54, 55]. Test results in these cases demonstrate that HELS can provide satisfactory reconstruction of the acoustic quantities even on an arbitrarily shaped surface with relatively few measurements in the low-to-mid frequencies and in particular, allow a piecewise or patch measurement and reconstruction.

Note that in conducting patch measurement at least one reference point should be selected. This reference point must not be moved in moving from one patch measurement to another.

It is worth noticing that since the expansion functions in the HELS formulations consist of the spherical wave functions, the solutions provided by Eqs. (3.66) and (3.67) converge very fast when measurement and reconstruction points are outside the minimum spherical surface that circumscribes an arbitrarily shaped source surface.

Inside this minimum spherical surface, however, the situation is unclear in the beginning. While numerous numerical and experimental results have confirmed the correctness of the HELS results inside this minimum spherical surface, the validity of HELS solutions was not established theoretically at first. Naturally, the validity of the HELS formulations inside the spherical surface that circumscribes arbitrary source geometry in an exterior region, or outside a maximum sphere that inscribes arbitrary source geometry in an interior region has been challenged when the HELS method was first introduced to the acoustics community.

Problems

3.1. Use the knowledge learned in Chap. 2 for the spherical Hankel functions and spherical harmonics and Eq. (3.4)–(3.12) to write the HELS expansion functions for $n = 3$ and 4.

3.2. Use Eq. (3.15) to reconstruct the acoustic pressure emitted by a dilating sphere of radius a. Suppose that the acoustic pressures measured at two arbitrary points r_1 and r_2 in space are $\hat{p}_1 = \rho_0 c \hat{v}_0 k a^2 e^{ik(r_1-a)}/[(ka+i)r_1]$ and $\hat{p}_2 = \rho_0 c \hat{v}_0 k a^2 e^{ik(r_2-a)}/[(ka+i)r_2]$, respectively. Find the acoustic pressure $\hat{p}(r, \theta, \phi; \omega)$ at any field point. Hint: use a one-term expansion in the HELS to reconstruct the radiated acoustic pressure field.

3.3. Continue Problem 3.2. Use Eq. (3.17) to reconstruct the normal component of the particle velocity $\hat{v}_n(r, \theta, \phi; \omega)$ at any field point based on the same measured acoustic pressures.

3.4. Use a two-term HELS expansion in Eq. (3.15) to reconstruct the acoustic pressure emitted by an oscillating sphere of radius a. Suppose that the input acoustic pressure at (r_1, θ_1, ϕ_1) is $\hat{p}_1 = \rho_0 c \hat{v}_0 k a^3 (k r_1 + i) e^{ik(r_1-a)}$

$\cos\theta_1/\left[\left(k^2a^2-2+i2ka\right)r_1^2\right]$ and that at $(r_2,\ \theta_2,\ \phi_2)$ is given by $\hat{p}_2=\rho_0 c\hat{v}_0 ka^3(kr_2+i)\mathrm{e}^{ik(r_2-a)}\cos\theta_2/\left[\left(k^2a^2-2+i2ka\right)r_2^2\right]$. Solve the acoustic pressure $\hat{p}(r,\theta,\phi;\omega)$ at any field point.

3.5. Continue Problem 3.4. Use Eq. (3.17) to reconstruct the normal component of the particle velocity $\hat{v}_n(r,\theta,\phi;\omega)$ at any field point based on the same measured acoustic pressures.

3.6. Use a two-term HELS expansion in Eq. (3.37) to predict the acoustic pressure emitted by an oscillating sphere of radius a. Suppose that the normal surface velocities at two arbitrary points on the surface of the sphere are given by $\hat{v}_{\mathrm{n}}(r_m,\theta_m,\phi_m;\omega)=V_z\cos\theta_m$, where $m=1$ and 2 and V_z is known.

3.7. Show that the errors in reconstructing the acoustic quantities on the source surface based on the acoustic pressures measured in the near field by using the HELS formulation (3.15) are of the order as given by Eq. (3.49).

3.8. Show that the errors in reconstructing acoustic quantities in the far field based on the near-field acoustic pressure measurements are of the order as given by Eq. (3.52).

3.9. Show that the errors in predicting the acoustic quantities on the source surface based on the near-field measurements by using the HELS formulation (3.44) are of the order as given by Eq. (3.55).

3.10. Show that the errors in predicting the acoustic quantities in the far field by using the HELS formulation (3.44) are of the order as given by Eq. (3.55).

3.11. Write a simple code for the HELS formulations to reconstruct the acoustic pressure fields based on the acoustic pressure input data. In this program the number of optimal terms in the HELS expansion should be specified automatically by the least-squares minimization process as given by Eq. (3.56).

3.12. Write a simple code for the HELS formulations to reconstruct the acoustic pressure fields based on the normal surface velocity input data. Once again, the number of optimal terms in the HELS expansion is specified automatically by using the least squares minimization process as given by Eq. (3.56).